
HIDDEN STATE DIFFERENTIAL PRIVATE MINI-BATCH BLOCK COORDINATE DESCENT FOR MULTI-CONVEXITY OPTIMIZATION

Ding Chen

Department of Computer Science

City University of Hong Kong

83 Tat Chee Avenue, Kowloon Tong, Hong Kong

ding.chen@my.cityu.edu.hk

Chen Liu

Department of Computer Science

City University of Hong Kong

83 Tat Chee Avenue, Kowloon Tong, Hong Kong

chen.liu@cityu.edu.hk

June 3, 2025

ABSTRACT

We investigate the differential privacy (DP) guarantees under the hidden state assumption (HSA) for multi-convex problems. Recent analyses of privacy loss under the hidden state assumption have relied on strong assumptions such as convexity, thereby limiting their applicability to practical problems. In this paper, we introduce the Differential Privacy Mini-Batch Block Coordinate Descent (DP-MBCD) algorithm, accompanied by the privacy loss accounting methods under the hidden state assumption. Our proposed methods apply to a broad range of classical non-convex problems which are or can be converted to multi-convex problems, such as matrix factorization and neural network training. In addition to a tighter bound for privacy loss, our theoretical analysis is also compatible with proximal gradient descent and adaptive calibrated noise scenarios.

1 Introduction

Machine learning has exhibited remarkable progress in the last decade across diverse fields. Their applications, such as recommendation systems Luo et al. [2014], image recognition He et al. [2016] and large language models Kandpal et al. [2022], have been integrated into people’s daily lives. However, the increasing demand for large amounts of training data in the training process has given rise to growing concerns regarding the potential privacy vulnerabilities [Fredrikson et al., 2015, Shokri et al., 2017] associated with the released models. For example, deep neural networks are shown to memorize the training data [Zhang et al., 2017] so that we can even reconstruct part of the training data from the learned model parameters [Haim et al., 2022]. To address these issues, differential privacy [Dwork, 2006] has become the gold standard for making formal and quantitative guarantees on model’s privacy and has been widely applied in learning problems [Abadi et al., 2016, Ha et al., 2019].

The predominate approach to ensuring differential privacy in the context of machine learning is Differential Private Stochastic Gradient Descent (DP-SGD) algorithm, which involves the incorporation of calibrated noise during each update step in the training phase. However, it also leads to a trade-off between utility and privacy guarantees [Allouah et al., 2023, Alvim et al., 2012]. Moreover, the privacy accounting method of DP-SGD Abadi et al. [2016] assumes that the algorithm’s internal states, i.e., the model’s parameters in each training step, can be revealed to the adversaries and are accounted to the privacy loss. As a result, the total privacy loss of the algorithm significantly increases with the number of training iterations, because more internal states will be revealed with more training iterations. Such assumptions lead to a very loose privacy estimation of the algorithm, because, in practice, most internal states are usually not even recorded during training. The gap between theory and practice motivates researchers to consider more realistic assumptions, which can not only boost the privacy guarantee for practical applications but also improve the utility-privacy trade-off.

Recently, the hidden state assumption was proposed to narrow down this gap [Chourasia et al., 2021, Feldman et al., 2018, Ye and Shokri, 2022, Altschuler and Talwar, 2022]. This assumption posits that the internal states of the training phase are hidden, and that the adversaries only have access to the states in the last iterate. Existing privacy enhancing

algorithms and the corresponding privacy accounting methods under the hidden state assumption [Feldman et al., 2018, Chourasia et al., 2021, Ye and Shokri, 2022, Altschuler and Talwar, 2022] are fundamentally contingent upon the properties of the loss function, such as strongly convexity. Although Chien and Li [2024] relax the assumption to (L, λ) Hölder's smoothness, it requires the exact L, λ of the loss function. The imposes significant limitations on their applicability, since we need to solve high-dimensional non-convex problems in most modern machine learning tasks.

In this paper, we propose a novel approach by integrating the privacy loss accountant with algorithm design, thereby providing tight privacy guarantee under the hidden state assumption with more relaxed assumptions for the loss function. Specifically, we consider the multi-convex loss functions and propose the *differential private mini-batch block coordinate descent* (DP-MBCD) algorithm with its privacy loss accountant methods under the hidden state assumption. Our methods apply to a broad range of popular in machine learning tasks such as recommendation systemLuo et al. [2014], low-rank matrix recoveryRecht et al. [2010] and neural network trainingZeng et al. [2019]. We summarize our contribution as follows:

- We consider multi-convex problems and propose *differentially private mini-batch block coordinate descent* (DP-MBCD), which, to the best of our knowledge, is the first feasible method to solve non-convex problems with non-trivial differential privacy guarantees under the hidden state assumption.
- The privacy analysis in this work possess a generic nature, rendering them compatible with proximal gradient descent and adaptive calibrated noise. Our privacy analysis also reveals that the convergence of privacy loss occurs due to the equilibrium solution that emerges when calibrated noise is fixed.
- By case study, we adapt our methods to two popular machine learning tasks: non-negative matrix factorization and neural network training. We demonstrate that our methods can achieve the tighter privacy guarantees under the hidden state assumption. Our methods thereby help practitioners develop privacy-enhancing techniques and boost model utility given the privacy constraints.

Terminology and Notation The privacy loss in this work refers to the *Rényi differential privacy* (RDP). When using the diffusion process to analyze the update scheme, we use t to represent the time in the process. We use $\|\cdot\|_2$ to represent l_2 norm for vectors and the spectral norm for matrices. In addition, $\|\cdot\|_F$ denotes Frobenius norm. Other notations are explicitly defined before usage. We summarize the definition of notations in Table 1 in Appendix A.

2 Related Works

Differential Privacy. Differential Privacy (DP) [Dwork, 2006] was initially introduced to quantitatively ensure the privacy guarantees within the realm of databases. Nevertheless, its rigorous mathematical foundations and nice properties, such as composition theorem and post-processing immunity, have raised more and more interest in its application in machine learning. Among the practical methods for achieving DP-guaranteed models, DP-SGD [Song et al., 2013] is the most popular one, which involves the addition of calibrated noise to the clipped per-sample gradients in each iterative update.

Besides the DP-guaranteed training algorithm, the proper accounting of privacy loss is also critical. Most accountant methods rely on the composition theorem of differential privacy. In this regard, Abadi et al. [2016] introduces the momentum accountant, Mironov [2017] further proposes Rényi differential privacy (RDP), which turns out a better tool to analyze the algorithm's privacy loss. Specifically, a randomized mechanism $\mathcal{M} : \mathcal{D} \rightarrow \mathcal{R}$ is said to have (α, ε) -RDP if for any adjacent datasets $d, d' \in \mathcal{D}$, it holds that $D_\alpha(\mathcal{M}(d) || \mathcal{M}(d')) \leq \varepsilon$ where D_α denotes the Rényi divergence of order α .

Hidden State Assumption. While the composition theorem assumes that adversaries have access to the intermediate states of the algorithm, which requires the summation of the privacy loss across each training iteration [Ponomareva et al., 2023], the hidden state assumption posits that these intermediate states remain concealed [Chourasia et al., 2021, Feldman et al., 2018, Ye and Shokri, 2022]. In real-life applications, the intermediate states usually cannot be tracked, so the hidden state assumption is more realistic. It is first proposed in Feldman et al. [2018], which proves that a sequence of contractive maps exhibit bounded (α, ε) -RDP. Subsequently, Chourasia et al. [2021] consider the update scheme of DP-GD as a Langevin diffusion process and analyze its privacy loss using the log-Sobolev inequality [Vempala and Wibisono, 2019]. Expanding upon this, Ye and Shokri [2022] analyze DP-SGD by leveraging the convergent analysis of unadjusted Langevin algorithm proposed by Wibisono [2019].

A more recent work Chien and Li [2024] provides the privacy loss accountant method for DP-SGD under the (L, λ) -Hölder's continuous gradient condition. However, its privacy loss accountant depends on the constant L, λ of the loss function, which is difficult to estimate. Therefore, as demonstrated in their opening problems parts, “several gaps

remain in neural network training". By contrast, our algorithm and privacy loss accountant can be applied to neural network training, as in our case studies.

Multi-Convexity. In a multi-convex optimization problem, variables can be partitioned into sets where the problem exhibits convexity with other variables fixed. Multi-convexity has been broadly studied in control Udell et al. [2016], machine learning Zeng et al. [2019], Gu et al. [2020] and signal processing Wen et al. [2012].

Block Coordinate Descent. Compared with gradient descent(GD), block coordinate descent (BCD) only updates part of the parameters and thus has lower memory consumption, making it suitable to train deep neural networks [Gu et al., 2020, Zeng et al., 2019, Zhang and Brand, 2017]. Zhang and Brand [2017] utilize a lifting trick to train deep neural networks with ReLU activations, which is then extended to more general activations Gu et al. [2020], Mangold et al. [2022a]. A more recent paper indicates that coordinate descent has the potential to find the global minimal of the neural network Akiyama.

BCD is also incorporated into some privacy-enhancement algorithms Damaskinos et al. [2021], Mangold et al. [2022b] with differential privacy guarantees. However, these works consider the privacy loss based on the composition theorem, which is based on pessimistic assumptions and leads to privacy loss overestimation. By contrast, we consider the more realistic hidden state assumption and mainly focus on the privacy loss accountant. Moreover, we also verify our result in both non-negative factorization and neural network training.

3 Preliminary

3.1 Private Multi-Convex Problem and Block Coordinate Descent

We consider a machine learning task formulated as the multi-convex optimization problem below:

$$\min_{\theta_{all} \in \vartheta, \phi_{all} \in \varphi} \mathcal{F}(\theta_{all}, \phi_{all}) \stackrel{\text{def}}{=} f(\theta_1, \dots, \theta_p, \phi_1, \dots, \phi_s) + r_\theta(\theta_1, \dots, \theta_p) + r_\phi(\phi_1, \dots, \phi_s) \quad (1)$$

In the given context, $\theta_{all} \stackrel{\text{def}}{=} \{\theta_i\}_{i=1}^p$ represents the released parameters, whereas $\phi_{all} \stackrel{\text{def}}{=} \{\phi_i\}_{i=1}^s$ denotes the hidden parameters. Released parameters may carry sensitive information and are potentially accessible to adversaries. Therefore, the differential privacy guarantee in this work is based on the released parameters. On the other hand, hidden parameters, such as auxiliary parameters, will not be stored or published. As a result, they do not pose any privacy concerns.

In this work, the set ϑ, φ are closed and block multi-convex, f is a differentiable and block multi-convex function, and r_θ, r_ϕ are extended-valued convex regularization functions that can be non-smooth. \mathcal{F} and f in Problem (1) represent the loss function.

If there is no ambiguity for notation simplicity, we only explicitly highlight the parameter we consider for function \mathcal{F} or f , with other parameters fixed. For example, $\mathcal{F}(\theta_j)$ means that we consider \mathcal{F} as a function on the block θ_j , with $\{\theta_i\}_{i=1, i \neq j}^p$ and $\{\phi_i\}_{i=1}^s$ fixed. Without loss of generality, we assume that f and \mathcal{F} are multi-convex on the blocks $\theta_1 \dots \theta_p$ and ϕ_1, \dots, ϕ_s . That is to say, $\mathcal{F}(\theta_i)$ and $f(\theta_i)$ is convex for each block θ_i ; $\mathcal{F}(\phi_i)$ and $f(\phi_i)$ is convex for each block ϕ_i . However, the function \mathcal{F} and f may be non-convex over the whole domain of θ_{all} and ϕ_{all} . Similarly, multi-convex set ϑ and φ mean their projections to each block θ_i and ϕ_i are convex, respectively.

In the realm of multi-convex optimization, the block coordinate descent (BCD) algorithm and its mini-batch block variant decomposes a large-scale optimization problem into several smaller convex subproblems for each block and has garnered significant popularity. We defer the pseudo-code and brief discussion of mini-batch block coordinate descent to Appendix B.1.

3.2 Case Study: Private Multi-Convex Optimization in Machine Learning Applications

A broad range of popular machine learning tasks can be formulated as multi-convex optimization problems. We investigate two examples below and demonstrate how they fit the framework discussed in the previous section.

Mini-batch Nonnegative Matrix Factorization: Mini-batch Nonnegative Matrix Factorization(MB-NMF), as a basic optimization problem, is widely used in recommendation systems Serizel et al. [2016]. Compared with classical Nonnegative Matrix Factorization (NMF), it offers significant advantages in handling large-scale and streaming data. MB-NMF solves the following optimization problem:

$$\min_{\mathbf{X} \geq 0, \mathbf{Y} \geq 0} \frac{1}{2} \|\mathbf{XY} - \mathbf{M}\|_F^2 + r_{\mathbf{X}}(\mathbf{X}) + r_{\mathbf{Y}}(\mathbf{Y}) \quad (2)$$

where $\mathbf{M} \in \mathbb{R}^{d_r \times d_c}$ is the input nonnegative matrix, $\mathbf{X} \in \mathbb{R}^{d_r \times d}$, $\mathbf{Y} \in \mathbb{R}^{d \times d_c}$ are the factorization results with $d \ll \min\{d_r, d_c\}$, $r_{\mathbf{X}}$ and $r_{\mathbf{Y}}$ are regularization functions promoting solution structures. In mini-batch updates, we stochastically select several rows of \mathbf{M} , update \mathbf{Y} and the corresponding rows of \mathbf{X} . The loss function in Problem (2) is non-convex in the domain of (\mathbf{X}, \mathbf{Y}) . However, it is multi-convex on the block \mathbf{X} and \mathbf{Y} , i.e., it is convex on \mathbf{X} with \mathbf{Y} fixed and on \mathbf{Y} with \mathbf{X} fixed. Regarding privacy concerns, released parameters or hidden parameters can be selectively and customarily determined based on specific requirements. In this paper, we assume that both \mathbf{X} and \mathbf{Y} may be available to adversaries, so they are released parameters. Therefore, Problem (2) that MB-NMF solves can be formulated in the framework of Problem (1).

Neural Network Training: We consider learning a D -layer feedforward neural network parameterized by its weight matrices $\mathbf{W} \stackrel{\text{def}}{=} \{\mathbf{W}_d\}_{d=0}^D$:

$$\min_{\mathbf{W}} \mathcal{L}(\mathbf{W}, \mathbf{x}_0) \stackrel{\text{def}}{=} \mathcal{R}(\mathbf{W}_D \mathbf{x}_D, y) + r(\mathbf{W}), \text{ s.t. } \mathbf{x}_{d+1} = \sigma_d(\mathbf{W}_d \mathbf{x}_d), \quad d = 0, \dots, D-1 \quad (3)$$

Here, (\mathbf{x}_0, y) is the input-label pair, \mathcal{R} is the loss function, such as the softmax cross-entropy function, r is the regularization function. Moreover, $\{\sigma_d\}_{d=0}^{D-1}$ are activation functions, such as ReLU function, that are Lipschitz continuous. Finally, weight matrices $\mathbf{W} \stackrel{\text{def}}{=} \{\mathbf{W}_d\}_{d=0}^D$ support fully-connected and convolutional layers. The loss function \mathcal{L} in Problem (3) is defined on one data instance for notation simplicity and can be straightforwardly extended to multiple data instances.

The loss function \mathcal{L} defined in Problem (3) is highly non-convex because of nonlinear activation functions, making it challenging for privacy accounting under the hidden state assumption. Nevertheless, we introduce auxiliary variables $\mathbf{u} \stackrel{\text{def}}{=} \{\mathbf{u}_d \stackrel{\text{def}}{=} \mathbf{W}_d \mathbf{x}_d\}_{d=0}^{D-1}$ [Zeng et al., 2019] and consider the Lagrangian function of Problem (3) with a multiplier co-efficient γ , which is set 1 in this work:

$$\mathcal{F}(\mathbf{W}, \mathbf{x}, \mathbf{u}) = \mathcal{R}(\mathbf{W}_D \mathbf{x}_D, y) + \frac{\gamma}{2} \sum_{d=0}^{D-1} (\|\mathbf{x}_{d+1} - \sigma_d(\mathbf{u}_d)\|_2^2 + \|\mathbf{u}_d - \mathbf{W}_d \mathbf{x}_d\|_2^2) + r(\mathbf{W}) \quad (4)$$

Here, we use $\mathbf{x} \stackrel{\text{def}}{=} \{\mathbf{x}_d\}_{d=0}^D$ to denote the post-activation value of each layer. In addition, we abuse the notation \mathcal{F} a little bit, since \mathcal{F} in Equation (4) is also a multi-convex function. Specifically, \mathcal{F} in Equation (4) is convex w.r.t. \mathbf{W} with \mathbf{x}, \mathbf{u} fixed, convex w.r.t. \mathbf{x} with \mathbf{W}, \mathbf{u} fixed and convex w.r.t. \mathbf{u} with \mathbf{W}, \mathbf{x} fixed. Moreover, the \mathbf{W} is the released parameters while the auxiliary variables \mathbf{x} and \mathbf{u} are hidden parameters because they are not saved in the trained model. Therefore, we can conclude that training neural networks by minimizing the Lagrangian function in Equation (4) can be formulated in the framework of Problem (1).

4 Differentially Private Mini-batch Block Coordinate Descent

We introduce differentially private mini-batch block coordinate descent (DP-MBCD) and the corresponding privacy accounting method in this section. DP-MBCD is generally applicable to multi-convex problems as discussed in Section 3.1, so we follow the notations as defined in Problem (1). Examples of machine learning problems discussed in Section 3.2 can be formulated as variants of Problem (1) where all the algorithms and analyses in this section are straightforwardly applicable.

4.1 Differentially Private Update Scheme

To leverage the multi-convex property of Problem (1), we design differentially private algorithms to solve Problem (1) based on block coordinate descent where $\theta_1, \dots, \theta_p$ and ϕ_1, \dots, ϕ_s are blocks. For hidden parameters ϕ_1, \dots, ϕ_s where privacy guarantees are not required, we directly compute the analytical or numerical solution for the block: $\forall i, \phi_i \leftarrow \arg \min_{\phi_i} f(\phi_i)$. For released parameters $\theta_1, \dots, \theta_p$ where we need differential privacy guarantees. We introduce calibrated noise and construct a Gaussian mechanism to protect privacy. Specifically, we approximate function f by its second-order Taylor expansion and derive the proximal gradient descent format for any released parameter block θ_i . Since the properties of the second-order derivative $\nabla^2 f$ are unknown, we introduce a hyper-parameter η as the step size instead.

$$\theta_i \leftarrow \arg \min_{\theta'_i} \langle \nabla f(\theta_i), \theta'_i - \theta_i \rangle + \frac{1}{2\eta} \|\theta'_i - \theta_i\|_F^2 + r_{\theta}(\theta'_i) = \text{Prox}_{\eta, r_{\theta}}(\theta_i - \eta \nabla f(\theta_i)) \quad (5)$$

Owing to the post-processing immunity, we add Gaussian calibrated noise inside the proximal operator to make the update differentially private. Furthermore, we propose calibrated noise with an adaptive variance to accommodate

different magnitudes of the gradient ∇f during training. As a result, we propose the following update scheme for each block of released parameters.

$$\boldsymbol{\theta}_i \leftarrow \text{Prox}_{\eta, r_{\boldsymbol{\theta}}} \left(\boldsymbol{\theta}_i - \eta \widetilde{\nabla f}(\boldsymbol{\theta}_i) + \mathcal{N}(0, 2\eta \cdot o(k, j) \mathbf{I}) \right) \quad (6)$$

where $o(k, j)$ is a function of the epoch index k and the iteration index j to control the magnitude of the calibrated noise, $\widetilde{\nabla f}(\boldsymbol{\theta}) = \min \left\{ \frac{\kappa \nabla f(\boldsymbol{\theta})}{\|\nabla^2 f(\boldsymbol{\theta})\|}, \nabla f(\boldsymbol{\theta}) \right\}$ introduces a hyper-parameter c to control the Lipschitz constants of the gradient descent update, which will be further explained in Section 4.2. By incorporating the update scheme (6) into MBCD (Algorithm 2 in Appendix B.1), we propose *differentially private mini-batch block coordinate descent (DP-MBCD)*, which is demonstrated in Algorithm 1 and will be proved to guarantee differential privacy in the next section.

Algorithm 1 Differentially Private mini-batch block coordinate descent(DP-MBCD)

```

1: Input: Training set, regularization terms  $\{r_d\}_{d=1}^D$ , learning rate  $\eta$ , batch size  $b$ 
2: Initialize parameters  $\boldsymbol{\theta}_{all}, \boldsymbol{\phi}_{all}$ 
3: for  $k = 1$  to  $K$  do
4:   for each mini-batch of size  $b$  do
5:      $\forall i = 1, \dots, s$ , update  $\boldsymbol{\phi}_i \leftarrow \arg \min_{\boldsymbol{\phi}_i} f(\boldsymbol{\phi}_i)$ .
6:      $\forall i = 1, \dots, p$ , update  $\boldsymbol{\theta}_i$  by (6) using stochastic gradient  $\nabla f$ .
7:   end for
8: end for

```

It is important to highlight that the DP-MBCD algorithm distinguishes itself from ℓ_2 -regularized gradient descent (as employed in Feldman et al. [2018], Ye and Shokri [2022]), where ℓ_2 regularization is essential to ensure strong convexity of the loss objective (e.g., Ye and Shokri [2022, Lemma 3.1], Feldman et al. [2018, Algorithm 1]). By contrast, in our framework, regularization is optional. Coordinate descent decomposes the original multi-convex problem into convex subproblems for each block, and the privacy accounting methods in the next section only requires convexity, in contrast to strongly convexity, for each subproblem. Additionally, the proximal term in our algorithm supports any convex regularization scheme like Lasso, thereby generalizing beyond ℓ_2 regularization.

Algorithm 1 provides a general framework for employing DP-MBCD to optimize multi-convex functions with differential privacy guarantee. In practice, the algorithm can be customized based on specific subproblems and the privacy loss accountant method. In Appendix B, we demonstrate Algorithm 3 for MB-NMF and Algorithm 4 for neural network training as customizations of Algorithm 1.

4.2 Privacy Accounting Analysis and Methods

We now study the privacy loss of Algorithm 1. Based on the post-processing immunity and composition property of differential privacy, we can establish an upper bound of the privacy loss of Algorithm 1 by summing the privacy losses of its sub-problems. Consequently, our primary focus here is to estimate the privacy loss associated with each sub-problem. For notation simplicity, we omit the subscript i in this subsection, as our analyses apply to any sub-problem for a block of released parameters. In addition, the privacy loss we derived for a block here does not depend on the value of any other blocks of released or hidden parameters because of the independency of each subproblem, so there is no inter-block privacy leakage.

We regard the update scheme (6) in Algorithm 1 as a diffusion process [Balle et al., 2019, Chourasia et al., 2021, Ye and Shokri, 2022]. Specifically, the update scheme consists of three steps: applying stochastic gradient descent $\boldsymbol{\theta} - \eta \nabla f(\boldsymbol{\theta})$, adding calibrated noise, and applying proximal operator associated with a convex regularization function $r_{\boldsymbol{\theta}}$. From a distributional perspective, let Θ be the distribution of the parameter $\boldsymbol{\theta}$, then the distribution of the parameter after one-step update in (6) can be represented by $\widetilde{\Theta}$ as follows:

$$\widetilde{\Theta} = T_{\#}(F_{\#}(\Theta) * \mathcal{N}(0, 2\eta \cdot o(k, j) \mathbf{I})), \quad F(\boldsymbol{\theta}) = \boldsymbol{\theta} - \eta \nabla f(\boldsymbol{\theta}), \quad T(\boldsymbol{\theta}) = \text{Prox}_{\eta, r_{\boldsymbol{\theta}}}(\boldsymbol{\theta}) \quad (7)$$

where $F_{\#}$ and $T_{\#}$ are two push-forward mappings. F represents the gradient descent update, T represents the proximal operator mapping, and $*$ represents the convolution operator between two distributions. Since f is multi-convex and $\boldsymbol{\theta}$ represents a block, $f(\boldsymbol{\theta})$ is convex. We then prove the Lipschitz continuity of the gradient descent update F , in which we clip the learning rate.

Lemma 4.1 (Lipschitz continuity for F). *Assume that $\beta \geq \nabla^2 f(\boldsymbol{\theta}) \geq 0$ and η is the learning rate and κ is the clipping threshold, the the update function $F(\boldsymbol{\theta}) = \boldsymbol{\theta} - \eta \widetilde{\nabla f}(\boldsymbol{\theta})$ where $\widetilde{\nabla f}(\boldsymbol{\theta}) = \min \left\{ \frac{\kappa \nabla f(\boldsymbol{\theta})}{\|\nabla^2 f(\boldsymbol{\theta})\|}, \nabla f(\boldsymbol{\theta}) \right\}$ is Lipschitz continuous with a constant $L_F \leq \max\{|1 - \kappa|, |1 - \eta\beta|\}$*

The proof is deferred to Appendix C.1. We highlight that the $f(\theta)$ in the Lemma 4.1 assumes that parameters except θ are fixed. In addition, the bound of the Lipschitz constant derived in Lemma 4.1 does not depend on any parameters, including both θ and other parameters. That is to say, any results derived from this bound do not leak any privacy.

Lemma 4.1 indicates that the Lipschitz constant L_F of function F depends on both the Hessian $\nabla^2 f(\theta)$ and the gradient clipping threshold κ . Hence, when customizing DP-MBCD to solve practical machine learning tasks, **we bound these two parameters to control the L_F** . For example, when solving NMF problems, we clip the gradient as in Algorithm 3. When training neural networks, inspired by normalization layer in Lemma B.1, we normalize each layer's output x_d to control the upper bound of $\nabla^2 f(\theta)$ in Algorithm 4. The normalization layer provides an efficient way to bound the local smoothness $\nabla^2 f(\theta)$, because it is time-consuming to calculate it directly.

Similarly, we can prove the Lipschitz continuity of the proximal operator in the update scheme (6).

Lemma 4.2 (Lipschitz continuity for T). *If $\eta > 0$ and $r_\theta(\theta)$ is a convex function, then the proximal operator function $T(\theta) = \text{Prox}_{\eta, r_\theta}(\theta) = \arg \min_{\tilde{\theta}} \left\{ r_\theta(\tilde{\theta}) + \frac{1}{2\eta} \|\tilde{\theta} - \theta\|_2^2 \right\}$ is Lipschitz continuous with a constant $L_T \leq 2$.*

The proof is deferred to Appendix C.2. Typical examples of the regularization function r_θ include 1) no regularization: $r_\theta(\theta) = 0$, and then $\text{Prox}_{\eta, r}(\theta) = \theta$; 2) l_2 regularization in weight decay: $r_\theta(\theta) = \frac{1}{2} \|\theta\|_2^2$, and then $\text{Prox}_{\eta, r_\theta}(\theta) = \frac{\eta}{1+\eta} \theta$; 3) l_1 regularization in LASSO: $r_\theta(\theta) = \|\theta\|_1$, and then $\text{Prox}_{\eta, r_\theta}(\theta) = \text{sign}(\theta) \cdot \max(0, |\theta| - \eta)$. In all these three cases, the proximal function is Lipschitz continuous and the Lipschitz constant is 1.

Now we assume that θ for each sub-problem satisfies the log-Sobolev inequality (LSI).

Definition 4.3. (Log-Sobolev Inequality Vempala and Wibisono [2019]) *A distribution ν over \mathbb{R}^d satisfies log-Sobolev inequality (LSI) with a constant c if \forall smooth function $g : \mathbb{R}^d \rightarrow \mathbb{R}$ with $\mathbb{E}_{\theta \sim \nu} [g^2(\theta)] < +\infty$,*

$$\mathbb{E}_{\theta \sim \nu} [g^2(\theta) \log(g^2(\theta))] - \mathbb{E}_{\theta \sim \nu} [g^2(\theta)] \log \mathbb{E}_{\theta \sim \nu} [g^2(\theta)] \leq \frac{2}{c} \mathbb{E}_{\theta \sim \nu} [\|\nabla g(\theta)\|_2^2] \quad (8)$$

LSI is a benign assumption commonly used in existing literature Vempala and Wibisono [2019], Ye and Shokri [2022] for the distribution of parameter. The formal definition of log-Sobolev inequality is provided in Definition C.1 in the appendix for reference. The LSI assumption is very mild, strongly log-concave distribution, such as Gaussian distribution, uniform distribution, and some non-logconcave distribution satisfy the LSI assumption Vempala and Wibisono [2019]. Based on the log-Sobolev inequality assumptions and Lipschitzness (Lemma 4.1, 4.2), we consider the recursive privacy dynamics for Equation (7) and bound the change rate of RDP during one step of noisy mini-batch proximal gradient descent. Our formal result is demonstrated as Theorem C.2 in Appendix C.3. It is an extension of Ye and Shokri [2022, Lemma 3.2] to the cases of non-convex loss functions, proximal gradient descent and adaptive calibrated noise.

To derive the privacy loss of Algorithm 1, we assume a bounded sensitivity of the total gradient for sub-problem $f(\theta)$, which is popular used in [Ye and Shokri, 2022, Das et al., 2023].

Assumption 4.4. (Sensitivity of the Total Gradient) *The l_2 sensitivity of the total gradient $\mathbb{E}_D \nabla f(\theta)$ is finite. That is to say, $\exists S_g < +\infty$ such that for any dataset D and its neighbouring dataset D' that only differs in one instance, we have $S_g = \max_{D, D', \theta} \|\mathbb{E}_D \nabla f(\theta) - \mathbb{E}_{D'} \nabla f(\theta)\|_2$.*

Based on bounded sensitivity, we apply Theorem C.2 to the case of two neighboring datasets and obtain the privacy loss of the Algorithm 1 for each iteration as in the following corollary. The proof is a variant of Ye and Shokri [2022, Lemma 3.2], so we omit it for the sake of brevity.

Corollary 4.5. *Under Assumption 4.4 where the sensitivity of the total gradient is $S_g < +\infty$, let D, D' be an arbitrary pair of the neighboring datasets that only differ in the i_0 -th data point (i.e. $x_{i_0} \neq x'_{i_0}$). Let B_k^j be a fixed mini-batch used in the j -th iteration of the k -th epoch in Algorithm 1, which contains b different training instances whose indices are sampled from $\{0, 1, \dots, n-1\}$. We denote θ_k^j and θ'^j_k as the intermediate parameters in Algorithm 1 when using datasets D and D' , respectively. If the distributions of θ_k^j and θ'^j_k satisfy log-Sobolev inequality with a constant c , the update function $F(\theta) = \theta - \eta \nabla f(\theta)$ and the proximal operator $T(\theta) = \text{Prox}_{\eta, r}(\theta)$ are Lipschitz continuous with Lipschitz constant L_F and L_T , respectively, then the following recursive bound for Rényi divergence holds for any order $\alpha > 1$:*

- 1) If $i_0 \notin B_k^j$, then $\frac{R_\alpha(\theta_k^{j+1} || \theta'^{j+1}_k)}{\alpha}$ is upper bounded by $\frac{R_{\alpha'}(\theta_k^j || \theta'^j_k)}{\alpha'} \cdot \left(1 + \frac{c \cdot 2\eta \cdot o(k, j)}{L_F^2}\right)^{-1/L_T^2}$ where the order $\alpha' = (\alpha - 1) \left(1 + \frac{c \cdot 2\eta o(k, j)}{L_F^2}\right)^{-1} + 1$.
- 2) If $i_0 \in B_k^j$, then $\frac{R_\alpha(\theta_k^{j+1} || \theta'^{j+1}_k)}{\alpha}$ is upper bounded by $\frac{R_\alpha(\theta_k^j || \theta'^j_k)}{\alpha} + \frac{\eta S_g^2}{4b^2 \cdot o(k, j)}$.

Compared with existing results Ye and Shokri [2022], Corollary 4.5 is first to demonstrate the influence of regularizer r_θ on the privacy loss through the Lipschitz constant L_T of the corresponding proximal operator. The smaller L_T^2 is, the better privacy guarantee will be obtained.

Corollary 4.5 concludes the change of the privacy loss for one iteration in Algorithm 1. By applying it iteratively, we can obtain the algorithm's privacy loss for the whole training phase. The formal theorem is demonstrated below.

Theorem 4.6. *Under Assumption 4.4 where the sensitivity of the total gradient is $S_g < +\infty$, the distribution of θ satisfies log-Sobolev inequality with a constant c . In addition, the update function $F(\theta) = \theta - \eta \nabla f(\theta)$ and the proximal operator $T(\theta) = \text{Prox}_{\eta, r}(\theta)$ are Lipschitz continuous with constants L_F and L_T , respectively. If we use Algorithm 4 to train model parameters θ for $K \geq 1$ epochs, then the algorithm satisfies $(\alpha, \varepsilon_K(\alpha))$ -Rényi differential privacy with the constant:*

$$\varepsilon_K(\alpha) \leq \frac{1}{\alpha - 1} \log \left(\sum_{j_0=0}^{n/b-1} \frac{b}{n} \cdot e^{(\alpha-1)(\varepsilon_K(\alpha, j_0))} \right)$$

where n is the size of the training set, b is the batch size, $\varepsilon_K(\alpha, j_0) \leq \sum_{k=0}^{K-1} \varepsilon_K(\alpha, j_0, k)$ and

$$\varepsilon_K(\alpha, j_0, k) = \alpha \cdot \frac{\eta S_g^2}{4b^2 \cdot o(k, j_0)} \cdot \left(\frac{c_k^{j_0+1}}{c_K^{n/b-1}} \left(\frac{1}{L_F^2 L_T^2} \right)^{(n/b-1)(K-k)-j_0} \prod_{l=k}^K \frac{c_l^{j_0+1}}{c_l^{j_0}} \right)^{-1/L_T^2} \quad (9)$$

In Equation (9), c_k^j is the log-Sobolev inequality constant for the distribution of the model parameters in the j -th iteration of the k -th epoch. Its value is calculated based on Lemma C.3 in Appendix C.4.

Proof Sketch. For each iteration of the Algorithm 1, the update scheme (6) fixed parameters except the θ . Hence, although the $f(\theta)$ in the update scheme differs among each iteration because of different fixed parameters, it maintains Lipschitzness in each iteration. Hence, we could use Corollary 4.5 to analyze the algorithm's privacy loss. In each epoch, there is one and only one different mini-batch for two neighboring datasets, so we assume it is the j_0 -th batch w.l.o.g. and apply case 2) of Corollary 4.5 for this mini-batch update and case 1) of Corollary 4.5 for the other updates. For any α , the original privacy loss is 0 and the recursive bound in Corollary 4.5 holds. Therefore, we can uniformly bounded the value of $\frac{\varepsilon_K(\alpha, j_0)}{\alpha}$ for any α . Finally, since j_0 is uniformly distributed among the index set $\{0, 1, \dots, n/b - 1\}$, we use the joint convexity of scaled exponentiation of Rényi divergence to bound the final privacy loss $\varepsilon_K(\alpha)$. The complete proof is deferred to the Appendix C.4.

$\varepsilon_K(\alpha, j_0)$ in the Theorem 4.6 represents the privacy loss when the only different instance of the two neighboring datasets is in the j_0 -th mini-batch of each epoch. The $\varepsilon_K(\alpha, j_0)$ shows that the overall privacy loss is the summation of each

epoch's privacy loss term $\frac{\eta S_g^2}{4b^2 \cdot o(k, j)}$ times a decay rate term $\left(\frac{c_k^{j_0+1}}{c_K^{n/b-1}} \left(\frac{1}{L_F^2 L_T^2} \right)^{(n/b-1)(K-k)-j_0} \prod_{l=k}^K \frac{c_l^{j_0+1}}{c_l^{j_0}} \right)^{-1/L_T^2}$.

More importantly, Algorithm 1 maintains the decay rate term smaller than 1 and decreases with the increase in K .

Theorem 4.6 improves the results in existing works from many aspects for estimating the differential privacy under hidden state assumptions. From a theoretical perspective, it is more generally applicable to different algorithms. Theorem 4.6 could easily extend the analyses and privacy guarantees from the gradient descent algorithm with calibrated noise from a fixed distribution to proximal gradient descent with adaptive calibrated noise. We will numerically show how Theorem 4.6 contributes to understanding the convergence of privacy loss in section 4.3. Second, when downgrading to the case of gradient descent with calibrated noise sampled from fixed distributions, Theorem 4.6 has a tighter bound than previous work Ye and Shokri [2022]. This is because we directly bound $\varepsilon_K(\alpha, j_0, k)$ by recursively applying Corollary 4.5. By contrast, Ye and Shokri [2022] approximates the upper bound of $\varepsilon_K(\alpha, j_0, k)$ in [Ye and Shokri, 2022, Theorem 3.3], which leads to inaccurate. Corollary 4.5 shows an exponential decrease in privacy loss, so such approximation affects the final privacy loss accountant, we draw a Figure in the Appendix E to indicate the difference.

In practice, Theorem 4.6 enables practical privacy accounting for multi-convex optimization: a critical advancement over existing results requiring strongly convexity, β -smoothness or (L, λ) Hölder smoothness. This theoretical breakthrough makes Algorithm 1 applicable to real-world non-convex problems including NMF and neural network training. We defer more details of algorithm customizations for different real-world tasks in Appendix B and numerical results in Appendix D.

4.3 Convergence of Privacy Loss and Noise Calibration

As discussed above, the bound of $\varepsilon_K(\alpha, j_0)$ in Theorem 4.6 demonstrates that the total privacy loss over K training epochs is a cumulative summation of per-epoch privacy losses under the hidden state assumption. Notably, each term in

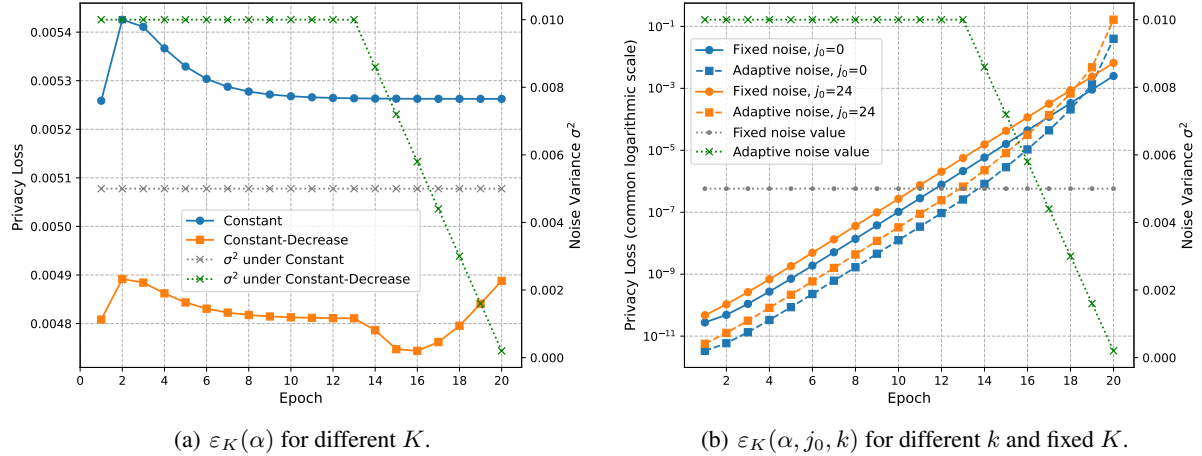


Figure 1: (a) We show the overall privacy loss $\varepsilon_K(\alpha)$ for different epoch numbers K . The horizontal axis represents K . (b) We show the privacy loss contribution $\varepsilon_K(\alpha, j_0, k)$ for the k -th epoch with a fixed epoch number $K = 20$ over different values of j_0 . The horizontal axis represent k and the left vertical axis is log-scale. The curves showing the variance of calibrated noise follow the right vertical axis. Hyper-parameters are as follow: Sensitivity $S_g = 1$, batch size $b = 100$ and sample size $n = 2500$, Lipschitzness $L_F = 0.98$, $L_T = 1$, learning rate $\eta = 0.05$, RDP order $\alpha = 10$

this summation consists of both a privacy loss component and a decay rate component, both of which depend on the variance of calibrated noise. Due to these interdependencies, deriving an analytical relationship between privacy loss and noise variance becomes challenging. Nevertheless, the framework of our algorithm and the privacy accounting methods support adaptive variance $o(k, j)$ of the calibrated noise. Therefore, we numerically explore how different choices of $o(k, j)$ for adaptive noise affects privacy loss. Figure 1(a) illustrates the privacy loss $\varepsilon_K(\alpha)$ under varying epoch number K . Figure 1(b) fix the epoch number K and demonstrate the privacy loss contribution of the k -th epoch $\varepsilon_K(\alpha, j_0, k)$ for different k , averaged over j_0 . Figure 1(b) indicates that the impact on the final privacy loss decays exponentially as states grow farther from the terminal state K . Moreover, when the calibrated noise is constant, we observe near-linear curves observed in the logarithmic scale graph, which suggests that the exponential decay has an approximately constant rate.

The observations in Figure 1 enhance our understanding of the *convergence of the privacy loss* under the hidden state assumption, initially proposed in Feldman et al. [2018]. More specifically, [Feldman et al., 2018, Theorem 23] directly get the converged privacy loss based on the Lipschitzness and use series a to allocate it. However, Theorem 4.6 indicates that if the exponential decay has a fixed rate, an equilibrium solution will emerge between the privacy loss and the decay rate after several epochs, resulting in the convergence of privacy loss under the hidden state assumption. However, adaptive noise calibration prevents such asymptotic stabilization by introducing an unstable decay rate, as shown in Figure 1(b). Figure 1(a) also supports these findings: privacy loss dynamics with constant noise display equilibrium tendencies. In contrast, when calibrated noise experiences a sharp increase at epoch 13, privacy loss with adaptive noise undergoes a significant phase. Furthermore, the observation motivates systematic exploration of adaptive noise strategies to achieve optimal utility-privacy trade-offs. While promising, rigorous analysis of algorithmic utility under such calibration exceeds our current scope and is deferred to future work.

5 Discussion and Future Works

General Applicability. Existing works study differential privacy under the hidden state assumption with strong assumptions on the loss functions, including strong convexity Feldman et al. [2018], Ye and Shokri [2022] and (L, λ) -Hölder smoothness Chien and Li [2024]. These assumptions limit their methods to apply to larger-scale and more complex machine learning tasks, such as training deep neural networks. By contrast, our work proposes a general framework of multi-convex optimization problem and DP-MBCD with non-trivial differential privacy guarantee under the hidden state assumption. To the best of our knowledge, our method is the first feasible method to training neural network in this context. Due to the page limit, we only list two examples of machine learning tasks to fit our framework in Section 3.2. In Appendix B, we demonstrate the generality of our framework by discussing more machine learning tasks with non-convex loss functions. We basically reformulate their non-convex loss functions into multi-convex optimization problem by introducing auxiliary variables. The effectiveness of our methods are validated by numerical experiments in Appendix D.

Comparison with DP-SGD. Although we provide the privacy loss comparison between DP-SGD under the composition theorem and DP-MBCD under the hidden state assumption for neural network training in Appendix D, it is crucial to note that direct comparisons of privacy loss can be misleading due to the differing threat models. Privacy loss under the hidden state assumption provides DP guarantees for the **distribution of published (final iteration) parameters**, whereas privacy loss under the composition theorem ensures DP guarantees for the **distribution of parameters at each iteration**. Consequently, the privacy loss under the hidden state assumption is predominantly influenced by the last few epochs, as demonstrated in Section 4.3, while the privacy loss under the composition theorem increases proportionally with the number of training iterations. Moreover, the DP-MBCD algorithm and the DP-SGD algorithm have entirely different parameter configurations, such as optimal step sizes and batch sizes, which play a significant role in both privacy loss accounting and the algorithm’s utility.

Further Extensions. Our algorithm can be extended in several ways to enhance its utility. For example, it can incorporate adaptive calibrated noise, variance reduction Ding and Li [2020, 2021], and large batch training techniques [Keskar et al., 2016, Hoffer et al., 2017]. These extensions depend on the convergence analysis of DP-MBCD. However, our paper primarily focuses on privacy loss analysis, which is separate from convergence analysis. We propose to explore these extensions in future work.

6 Conclusion

We introduce the *Differentially Private mini-batch block coordinate descent* (DP-MBCD) algorithm, which incorporates proximal gradient descent and adaptive noise for multi-convexity optimization. To the best of our knowledge, DP-MBCD is the first algorithm capable of addressing non-convex problems such as neural network training while ensuring a tight differential privacy guarantee under the hidden state assumption. Our theoretical analysis reveals varying privacy loss contributions across different training phases under the hidden state assumption, explaining the reason of the convergence of privacy loss and inspiring adaptive noise calibration during training. Moreover, our experiments indicate that adaptive noise allows adjustable trade-offs between model utility and privacy.

References

Xin Luo, Mengchu Zhou, Yunni Xia, and Qingsheng Zhu. An efficient non-negative matrix-factorization-based approach to collaborative filtering for recommender systems. *IEEE Transactions on Industrial informatics*, 10(2):1273–1284, 2014.

Kaiming He, Xiangyu Zhang, Shaoqing Ren, and Jian Sun. Deep residual learning for image recognition. In *Proceedings of the IEEE conference on computer vision and pattern recognition*, pages 770–778, 2016.

Nikhil Kandpal, Eric Wallace, and Colin Raffel. Deduplicating training data mitigates privacy risks in language models. In *International Conference on Machine Learning*, pages 10697–10707. PMLR, 2022.

Matt Fredrikson, Somesh Jha, and Thomas Ristenpart. Model inversion attacks that exploit confidence information and basic countermeasures. In *Proceedings of the 22nd ACM SIGSAC conference on computer and communications security*, pages 1322–1333, 2015.

Reza Shokri, Marco Stronati, Congzheng Song, and Vitaly Shmatikov. Membership inference attacks against machine learning models. In *2017 IEEE symposium on security and privacy (SP)*, pages 3–18. IEEE, 2017.

Chiyuan Zhang, Samy Bengio, Moritz Hardt, Benjamin Recht, and Oriol Vinyals. Understanding deep learning requires rethinking generalization. In *International Conference on Learning Representations*, 2017. URL <https://openreview.net/forum?id=Sy8gdB9xx>.

Niv Haim, Gal Vardi, Gilad Yehudai, Ohad Shamir, and Michal Irani. Reconstructing training data from trained neural networks. *Advances in Neural Information Processing Systems*, 35:22911–22924, 2022.

Cynthia Dwork. Differential privacy. In *International colloquium on automata, languages, and programming*, pages 1–12. Springer, 2006.

Martin Abadi, Andy Chu, Ian Goodfellow, H Brendan McMahan, Ilya Mironov, Kunal Talwar, and Li Zhang. Deep learning with differential privacy. In *Proceedings of the 2016 ACM SIGSAC conference on computer and communications security*, pages 308–318, 2016.

Trung Ha, Tran Khanh Dang, Tran Tri Dang, Tuan Anh Truong, and Manh Tuan Nguyen. Differential privacy in deep learning: an overview. In *2019 International Conference on Advanced Computing and Applications (ACOMP)*, pages 97–102. IEEE, 2019.

Youssef Allouah, Rachid Guerraoui, Nirupam Gupta, Rafael Pinot, and John Stephan. On the privacy-robustness-utility trilemma in distributed learning. In Andreas Krause, Emma Brunskill, Kyunghyun Cho, Barbara Engelhardt, Sivan Sabato, and Jonathan Scarlett, editors, *Proceedings of the 40th International Conference on Machine Learning*, volume 202 of *Proceedings of Machine Learning Research*, pages 569–626. PMLR, 23–29 Jul 2023. URL <https://proceedings.mlr.press/v202/allouah23a.html>.

Mário S Alvim, Miguel E Andrés, Konstantinos Chatzikokolakis, Pierpaolo Degano, and Catiuscia Palamidessi. Differential privacy: on the trade-off between utility and information leakage. In *Formal Aspects of Security and Trust: 8th International Workshop, FAST 2011, Leuven, Belgium, September 12-14, 2011. Revised Selected Papers 8*, pages 39–54. Springer, 2012.

Rishav Chourasia, Jiayuan Ye, and Reza Shokri. Differential privacy dynamics of langevin diffusion and noisy gradient descent. *Advances in Neural Information Processing Systems*, 34:14771–14781, 2021.

Vitaly Feldman, Ilya Mironov, Kunal Talwar, and Abhradeep Thakurta. Privacy amplification by iteration. In *2018 IEEE 59th Annual Symposium on Foundations of Computer Science (FOCS)*, pages 521–532. IEEE, 2018.

Jiayuan Ye and Reza Shokri. Differentially private learning needs hidden state (or much faster convergence). *Advances in Neural Information Processing Systems*, 35:703–715, 2022.

Jason Altschuler and Kunal Talwar. Privacy of noisy stochastic gradient descent: More iterations without more privacy loss. *Advances in Neural Information Processing Systems*, 35:3788–3800, 2022.

Eli Chien and Pan Li. Convergent privacy loss of noisy-sgd without convexity and smoothness. *arXiv preprint arXiv:2410.01068*, 2024.

Benjamin Recht, Maryam Fazel, and Pablo A Parrilo. Guaranteed minimum-rank solutions of linear matrix equations via nuclear norm minimization. *SIAM review*, 52(3):471–501, 2010.

Jinshan Zeng, Tim Tsz-Kit Lau, Shaobo Lin, and Yuan Yao. Global convergence of block coordinate descent in deep learning. In *International conference on machine learning*, pages 7313–7323. PMLR, 2019.

Shuang Song, Kamalika Chaudhuri, and Anand D Sarwate. Stochastic gradient descent with differentially private updates. In *2013 IEEE global conference on signal and information processing*, pages 245–248. IEEE, 2013.

Ilya Mironov. Rényi differential privacy. In *2017 IEEE 30th computer security foundations symposium (CSF)*, pages 263–275. IEEE, 2017.

Natalia Ponomareva, Hussein Hazimeh, Alex Kurakin, Zheng Xu, Carson Denison, H Brendan McMahan, Sergei Vassilvitskii, Steve Chien, and Abhradeep Guha Thakurta. How to dp-fy ml: A practical guide to machine learning with differential privacy. *Journal of Artificial Intelligence Research*, 77:1113–1201, 2023.

Santosh Vempala and Andre Wibisono. Rapid convergence of the unadjusted langevin algorithm: Isoperimetry suffices. *Advances in neural information processing systems*, 32, 2019.

Andre Wibisono. Proximal langevin algorithm: Rapid convergence under isoperimetry. *arXiv preprint arXiv:1911.01469*, 2019.

Madeleine Udell, Corinne Horn, Reza Zadeh, Stephen Boyd, et al. Generalized low rank models. *Foundations and Trends® in Machine Learning*, 9(1):1–118, 2016.

Fangda Gu, Armin Askari, and Laurent El Ghaoui. Fenchel lifted networks: A lagrange relaxation of neural network training. In *International Conference on Artificial Intelligence and Statistics*, pages 3362–3371. PMLR, 2020.

Zaiwen Wen, Wotao Yin, and Yin Zhang. Solving a low-rank factorization model for matrix completion by a nonlinear successive over-relaxation algorithm. *Mathematical Programming Computation*, 4(4):333–361, 2012.

Ziming Zhang and Matthew Brand. Convergent block coordinate descent for training tikhonov regularized deep neural networks. *Advances in Neural Information Processing Systems*, 30, 2017.

Paul Mangold, Aurélien Bellet, Joseph Salmon, and Marc Tommasi. Differentially private coordinate descent for composite empirical risk minimization. In Kamalika Chaudhuri, Stefanie Jegelka, Le Song, Csaba Szepesvari, Gang Niu, and Sivan Sabato, editors, *Proceedings of the 39th International Conference on Machine Learning*, volume 162 of *Proceedings of Machine Learning Research*, pages 14948–14978. PMLR, 17–23 Jul 2022a.

Shunta Akiyama. Block coordinate descent for neural networks provably finds global minima.

Georgios Damaskinos, Celestine Mendler-Dünner, Rachid Guerraoui, Nikolaos Papandreou, and Thomas Parnell. Differentially private stochastic coordinate descent. In *Proceedings of the AAAI Conference on Artificial Intelligence*, volume 35, pages 7176–7184, 2021.

Paul Mangold, Aurélien Bellet, Joseph Salmon, and Marc Tommasi. Differentially private coordinate descent for composite empirical risk minimization. In *International Conference on Machine Learning*, pages 14948–14978. PMLR, 2022b.

Romain Serizel, Slim Essid, and Gaël Richard. Mini-batch stochastic approaches for accelerated multiplicative updates in nonnegative matrix factorisation with beta-divergence. In *2016 IEEE 26th International Workshop on Machine Learning for Signal Processing (MLSP)*, pages 1–6. IEEE, 2016.

Borja Balle, Gilles Barthe, Marco Gaboardi, and Joseph Geumlek. Privacy amplification by mixing and diffusion mechanisms. *Advances in neural information processing systems*, 32, 2019.

Rudrajit Das, Satyen Kale, Zheng Xu, Tong Zhang, and Sujay Sanghavi. Beyond uniform lipschitz condition in differentially private optimization. In *International Conference on Machine Learning*, pages 7066–7101. PMLR, 2023.

Zhiyan Ding and Qin Li. Variance reduction for random coordinate descent-langevin monte carlo. *Advances in Neural Information Processing Systems*, 33:3748–3760, 2020.

Zhiyan Ding and Qin Li. Langevin monte carlo: random coordinate descent and variance reduction. *Journal of machine learning research*, 22(205):1–51, 2021.

Nitish Shirish Keskar, Dheevatsa Mudigere, Jorge Nocedal, Mikhail Smelyanskiy, and Ping Tak Peter Tang. On large-batch training for deep learning: Generalization gap and sharp minima. *arXiv preprint arXiv:1609.04836*, 2016.

Elad Hoffer, Itay Hubara, and Daniel Soudry. Train longer, generalize better: closing the generalization gap in large batch training of neural networks. *Advances in neural information processing systems*, 30, 2017.

Zitao Li, Bolin Ding, Ce Zhang, Ninghui Li, and Jingren Zhou. Federated matrix factorization with privacy guarantee. *Proceedings of the VLDB Endowment*, 15(4), 2021.

Jimmy Lei Ba, Jamie Ryan Kiros, and Geoffrey E Hinton. Layer normalization. *arXiv preprint arXiv:1607.06450*, 2016.

Leo P Kadanoff. *Statistical physics: statics, dynamics and renormalization*. World Scientific, 2000.

Yangyang Xu and Wotao Yin. A block coordinate descent method for regularized multiconvex optimization with applications to nonnegative tensor factorization and completion. *SIAM Journal on imaging sciences*, 6(3):1758–1789, 2013.

Zhiqi Bu, Yu-Xiang Wang, Sheng Zha, and George Karypis. Differentially private optimization on large model at small cost. In *International Conference on Machine Learning*, pages 3192–3218. PMLR, 2023.

Zhiqi Bu, Yu-Xiang Wang, Sheng Zha, and George Karypis. Automatic clipping: Differentially private deep learning made easier and stronger. *Advances in Neural Information Processing Systems*, 36, 2024.

Isabelle Guyon, Steve Gunn, Asa Ben-Hur, and Gideon Dror. Result analysis of the nips 2003 feature selection challenge. *Advances in neural information processing systems*, 17, 2004.

A Notation Table

Symbol	Meaning	Where
θ_{all}	Released parameters	Eq. 1
ϕ_{all}	Hidden parameters	Eq. 1
ϑ, φ	Closed block multi-convex sets	Subsec. 3.1
$\mathcal{F}(\theta_{all}, \phi_{all})$	Loss function	Eq. 1
$f(\theta_{all}, \phi_{all})$	Loss function without regularization	Eq. 1
$f(\theta)$	Loss functions with respect to θ with other parameters fixed and without regularization term.	Eq. 1
$\mathcal{F}(\theta)$	Loss functions with respect to θ with other parameters fixed.	Eq. 1
$\mathcal{F}_b(\theta), f_b(\theta)$	$\mathcal{F}(\theta)$ and $f_b(\theta)$ with mini batch input, where batch size is b	Eq. 1
r_θ, r_ϕ	Convex regularization functions	Eq. 1
\mathbf{M}	Input nonnegative matrix for NMF problem	Eq. 2
\mathbf{X}, \mathbf{Y}	Matrix factorization results for NMF problem	Eq. 2
\mathbf{W}	Neural network weight matrices	Eq. 3
\mathcal{R}	Loss function (e.g., cross-entropy) For Neural Network Training	Eq. 3
y	Label in neural network	Eq. 3
\mathbf{x}_0	Input data in neural network	Eq. 3
σ_d	d -th layer's Activation functions	Eq. 3
\mathbf{u}, \mathbf{x}	Auxiliary variables	Eq. 4
η	Learning rate	Eq. 5
κ	Clipping threshold	Eq. 6
$o(k, j)$	Noise magnitude control function	Eq. 6
α	Rényi divergence order	Def. C.1
S_g	Total gradient sensitivity	Assumption 4.4
K	Total number of training epochs	Alg. 1
j_0	Index of mini-batch containing differing data instance	Cor. 4.5
c	Log-Sobolev inequality (LSI) constant	Def. C.1
c_k^j	LSI constant at j -th iteration of k -th epoch	Lem. C.3
n	Size of training dataset	Sec. 4.2
b	Mini-batch size	Alg. 1

Table 1: Symbol Table For Algorithms and Definitions

B Additional Algorithms

B.1 Mini-Batch Block Coordinate Descent

The pseudo-code of mini-batch block coordinate descent for solving Problem (1) is shown as follows. In practice, we can also update the block $\{\theta_i\}_{i=1}^p, \{\phi_i\}_{i=1}^s$ alternatively. When $\arg \min_{\phi_i} \mathcal{F}(\phi_i)$ or $\arg \min_{\theta_i} \mathcal{F}(\theta_i)$ is difficult to solve, we may use gradient-based methods to obtain the approximate optimal values instead.

Algorithm 2 Mini-Batch Block Coordinate Descent (MBCD)

- 1: **Input:** Training set, regularization terms r_θ, r_ϕ , batch size b , number of epochs K .
- 2: Initialize parameters θ_{all}, ϕ_{all}
- 3: **for** $k = 1$ to K **do**
- 4: **for** each mini-batch of size b **do**
- 5: $\forall i = 1, \dots, p$, update $\phi_i \leftarrow \arg \min_{\phi_i} \mathcal{F}(\phi_i)$
- 6: $\forall i = 1, \dots, s$, update $\theta_i \leftarrow \arg \min_{\theta_i} \mathcal{F}(\theta_i)$
- 7: **end for**
- 8: **end for**

B.2 DP-MBCD Adaptations for Specific Machine Learning Tasks

Algorithm 1 provides a general framework for multi-convex function. It will be customized to solve specific optimization problems in various machine learning tasks. In this section, we discuss detailed algorithms in solving the NMF problem and neural network training which we discuss in the case study in Section 3.2.

B.2.1 Algorithm for NMF

Unlike deep learning scenarios, which use several batches of data to update the same set of parameters in neural networks, the parameters of an NMF problem, i.e., \mathbf{X} and \mathbf{Y} in Problem (2), are highly correlated to the individual data. Taking the recommendation system task as an example: a recommendation system typically involves a $d_r \times d_c$ rating matrix \mathbf{M} , where d_r denotes users and d_c represents items (e.g., products, movies, or services), with $M_{r,c}$ indicating user r 's rating on item c . The core objective is to approximate this sparse matrix via NMF, which aims to extract low-rank user embeddings $\mathbf{X} \in \mathbb{R}^{d_r \times d}$ and item embeddings $\mathbf{Y} \in \mathbb{R}^{d \times d_c}$ such that $\mathbf{XY} \approx \mathbf{M}$.

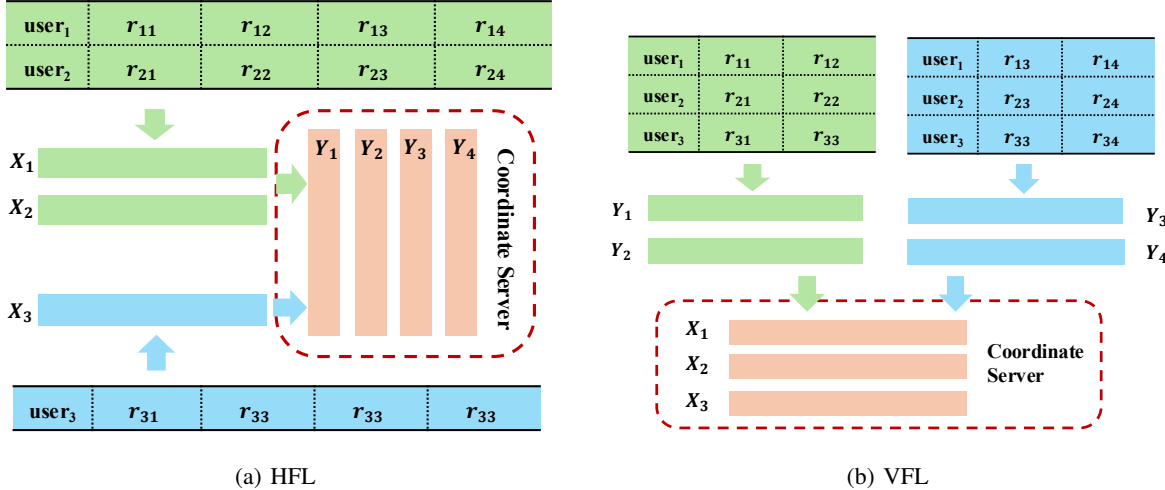


Figure 2: (a) Horizontal Federate Learning (HFL). (b) Vertical Federate Learning (VFL). For Horizontal Federate Learning, we assume each node provide private user's rating data. For Vertical Federate Learning, we assume each node provide private ranking data for different items.

Regarding privacy concerns, specific data's privacy matters more than the whole matrix. Therefore, we use mini-batches to provide privacy guarantees for specific data. For example, Figure 2 shows VFL (vertical federated learning) and HFL (horizontal federated learning) proposed by Li et al. [2021]. In HFL, each \mathbf{X}_i indicates user's rating information and can be stored in different nodes. In practice, it means several companies have different users' ranking information or different users have different privacy preference for their data. By contrast, \mathbf{Y} as a whole is stored in the centralized coordinate server and contains the information for all items. Correspondingly, the privacy loss can also be decomposed into two parts: user-level privacy loss $\varepsilon_{\mathbf{X}_i}$ for each user and the overall item-level privacy loss $\varepsilon_{\mathbf{Y}}$. Therefore, the total privacy loss for HFL should be $\varepsilon_H = \max\{\varepsilon_{\mathbf{X}_1}, \dots, \varepsilon_{\mathbf{X}_i}\} + \varepsilon_{\mathbf{Y}}$. Similarly, for VFL, each term's information \mathbf{Y}_j may be stored in different nodes while \mathbf{X} as a whole is stored in the centralized coordinate server and contain the information for all users. Hence, the privacy loss calculation for VFL should be $\varepsilon_V = \max\{\varepsilon_{\mathbf{Y}_1}, \dots, \varepsilon_{\mathbf{Y}_j}\} + \varepsilon_{\mathbf{X}}$.

For simplicity, we do not consider the regularization term and propose Algorithm 3. In our algorithm, we divided the matrix \mathbf{M} horizontally, which means we consider the HFL case.

B.2.2 Algorithm for Neural Network Training

In neural network training, i.e., Problem (3), auxiliary parameters $\mathbf{x} \stackrel{\text{def}}{=} \{\mathbf{x}_d\}_{d=1}^D$ and $\mathbf{u} \stackrel{\text{def}}{=} \{\mathbf{u}_d\}_{d=0}^{D-1}$ are hidden, while neural network parameters $\mathbf{W} \stackrel{\text{def}}{=} \{\mathbf{W}_d\}_{d=0}^D$ are released. Hence, we do not need privacy enhancement technique like Equation (6) to update \mathbf{x} and \mathbf{u} .

Algorithm 3 Differential Private Block Coordinate Descent For NMF

Input: Ranking matrix \mathbf{M} , learning rate η , clipping threshold κ , gradient sensitivity S_g , number of epochs K , batch size b .
Initialization: \mathbf{X}, \mathbf{Y} .
for epoch $k = 1, 2, \dots, K$ **do**
 for each mini-batch of size b indexed by i **do**
 // Update \mathbf{X}
 $g_{\mathbf{X}} = ([\mathbf{XY}]_i - [\mathbf{M}]_i) [\mathbf{Y}]_i^T$
 $g_{\mathbf{X}} \leftarrow g_{\mathbf{X}} \cdot \min\{1, S_g/\|g_{\mathbf{X}}\|\}$ ▷ Bounding gradient sensitivity(Assumption 4.4)
 $h_{\mathbf{X}} \leftarrow [\mathbf{YY}^T]_i \cdot \min\{1, S_g/\|g_{\mathbf{X}}\|\}$ ▷ Bounding gradient Lipschitz(Lemma 4.1)
 $\mathbf{X} \leftarrow \mathbf{X} - \eta(g_{\mathbf{X}} \cdot \min\{1, \kappa/\|h_{\mathbf{X}}\|_2\}) + \sqrt{2\eta}\mathcal{N}(0, o(k, j))$.
 end for
 // Update \mathbf{Y}
 $g_{\mathbf{Y}} \leftarrow g_{\mathbf{Y}} \cdot \min\{1, S_g/\|g_{\mathbf{Y}}\|\}$ ▷ Bounding gradient sensitivity(Assumption 4.4)
 $h_{\mathbf{Y}} \leftarrow \mathbf{XX}^T \cdot \{1, S_g/\|g_{\mathbf{Y}}\|\}$ ▷ Bounding gradient Lipschitz(Lemma 4.1)
 $\mathbf{Y} \leftarrow \mathbf{Y} - \eta(g_{\mathbf{Y}} \cdot \min\{1, \kappa/\|h_{\mathbf{Y}}\|_2\}) + \sqrt{2\eta}\mathcal{N}(0, o(k, j))$.
end for

To update \mathbf{u} , we consider the ReLU activation function and utilize Zeng et al. [2019, Lemma 13] as follows to obtain the analytical solution.

$$\forall d, \quad \mathbf{u}_d \leftarrow \begin{cases} \mathbf{W}_d \mathbf{x}_d & \text{if } -\mathbf{x}_{d+1} \leq \mathbf{W}_d \mathbf{x}_d \leq -(\sqrt{2} - 1)\mathbf{x}_{d+1} \leq 0. \\ \min\{0, \mathbf{W}_d \mathbf{x}_d\} & \text{if } \mathbf{W}_d \mathbf{x}_d + \mathbf{x}_{d+1} \leq 0. \\ \frac{1}{2}(\mathbf{W}_d \mathbf{x}_d + \mathbf{x}_{d+1}) & \text{otherwise.} \end{cases} \quad (10)$$

To update \mathbf{x} , we have the analytical solution due to the convexity of $\mathcal{F}(\mathbf{x})$.

$$\forall d, \quad \mathbf{x}_d \leftarrow \begin{cases} (\mathbf{W}_d^T \mathbf{W}_d + \mathbf{I})^{-1} (\mathbf{W}_d^T \mathbf{u}_d + \sigma(\mathbf{u}_{d-1})) & \text{if } d = 0, 1, \dots, D-1. \\ \text{Prox}_{\frac{1}{\gamma}, \mathcal{R}}(\sigma_{d-1}(\mathbf{u}_{d-1})). & \text{if } d = D \end{cases} \quad (11)$$

Additionally, inspired by the layer normalization Ba et al. [2016], we clip the auxiliary variables \mathbf{x} by the threshold ρ_d . We control the magnitude of \mathbf{x} to enforce the Lipschitz smoothness of $\mathcal{F}(\mathbf{W})$.

$$\forall d, \quad \mathbf{x}_d \leftarrow \mathbf{x}_d \cdot \min(\rho_d/\|\mathbf{x}_d\|_2, 1) \quad (12)$$

Normalization as shown in Equation (12) is necessary to guarantee the privacy of the released variables \mathbf{W} , which is further discussed in Lemma B.1 below.

Lemma B.1. [Lipschitz continuity for \mathbf{W} update] For d -th layer, the update function $F(\mathbf{W}) = \mathbf{W} - \eta \nabla f(\mathbf{W})$ is Lipschitz continuous with $L_F = |1 - \gamma \eta \rho_d^2|$

Proof. We first consider the Lipschitz smoothness factor for each layer $f(\mathbf{W}_d) = \frac{\gamma}{2} \|\mathbf{u}_d - \mathbf{W}_d \mathbf{x}_d\|_F^2$. We first calculate the gradient of $f(\mathbf{W}_d)$ as follows:

$$\nabla f(\mathbf{W}_d) = \gamma(\mathbf{U}_d - (\mathbf{W}_d \mathbf{x}_d)) \mathbf{x}_d^T$$

where \mathbf{x}_d and \mathbf{U}_d is fixed. Therefore, $\nabla f(\mathbf{W}_d)$, we have the following bound:

$$\|\nabla f(\mathbf{W}_d) - \nabla f(\mathbf{W}'_d)\|_2 \leq \gamma \|\mathbf{x}_d\|_2^2 \|\mathbf{W}_d - \mathbf{W}'_d\|_2 \quad (13)$$

Therefore, $f(\mathbf{W}_d)$ as a function of \mathbf{W}_d is Lipschitz smooth with a factor $\gamma \rho_d^2$. Based on this, it is straightforward that the update function is Lipschitz continuous with a constant $L_F = |1 - \gamma \eta \rho_d^2|$. \square

Lemma B.1 indicates that the Hessian spectrum $|\nabla^2 f(\mathbf{W})|$ is bounded by $\gamma \rho_d^2$. Therefore, it becomes unnecessary to control the Hessian spectrum to calculate $\widetilde{\nabla} f$ as in Equation (6). In other words, the gradient sensitivity $S_g = \gamma \rho_d^2$, and we can directly use the gradient to update \mathbf{W} as follows:

$$\forall d, \quad \mathbf{W}_d \leftarrow \text{Prox}_{\eta, r_{\theta}}(\mathbf{W}_d - \eta \nabla f(\mathbf{W}_d) + \mathcal{N}(0, 2\eta \cdot o(k, j) \mathbf{I})) \quad (14)$$

Hence, for neural network training, we demonstrate DP-MBCD as Algorithm 4, where we set $\gamma = 1$ in this paper.

Implementation on Convolutional Neural Network: The algorithm 4 can be also applied to CNN since the convolution operator can also be regard as a linear operations. More specifically, we could use the image to column algorithm to

Algorithm 4 Differentially Private Mini-Batch Block Coordinate Descent For Neural Networks

Input: training set, regularization schemes r_{θ} , step size η , batch size b , number of epochs K , noise control function $o(k, j)$, clipping threshold ρ_d .

Initialization: $\mathbf{W} \stackrel{\text{def}}{=} \{\mathbf{W}_d\}_{d=0}^D, \mathbf{x} \stackrel{\text{def}}{=} \{\mathbf{x}_d\}_{d=0}^D, \mathbf{u} \stackrel{\text{def}}{=} \{\mathbf{u}_d\}_{d=0}^{D-1}$.

for epoch $k = 1, 2, \dots, K$ **do**

for each mini-batch of size b **do**

$\forall d$, update $\mathbf{x}_d \leftarrow \arg \min_{\mathbf{x}'_d} \mathcal{F}(\mathbf{x}'_d)$ based on Equation (11) and then clip \mathbf{x}_d by Equation (12).

$\forall d$, update $\mathbf{u}_d \leftarrow \arg \min_{\mathbf{u}'_d} \mathcal{F}(\mathbf{u}'_d)$ based on Equation (10).

$\forall d$, update \mathbf{W}_d based on Equation (14).

end for

end for

convert the $\mathbf{W} * \mathbf{x}$ to $\mathbf{W}\mathbf{x}$. Moreover, in solving the sub-problem $f(\mathbf{x})$, we need to convert $\mathbf{W} * \mathbf{x}$ to $\mathbf{W}\mathbf{x}$ where \mathbf{x} need to be flatten as a vector and generate the Toeplitz matrix. We take a 3×3 input \mathbf{x} with a 2×2 kernel \mathbf{W} , with stride equals 1 where x, w is the element in matrix \mathbf{W}, \mathbf{x} . For example, if we convert the \mathbf{x}_d to a vector and the Toeplitz for \mathbf{W} is as follow:

$$\begin{bmatrix} w_{11} & w_{12} & 0 & w_{21} & w_{22} & 0 & 0 & 0 & 0 \\ 0 & w_{11} & w_{12} & 0 & w_{21} & w_{22} & 0 & 0 & 0 \\ 0 & 0 & 0 & w_{11} & w_{12} & 0 & w_{21} & w_{22} & 0 \\ 0 & w_{11} & w_{12} & 0 & w_{21} & w_{22} & 0 & 0 & 0 \end{bmatrix} * \begin{bmatrix} x_{11} \\ x_{12} \\ x_{13} \\ x_{21} \\ x_{22} \\ x_{23} \\ x_{31} \\ x_{32} \\ x_{33} \end{bmatrix}$$

The Variant of Algorithm 4: We scale down the update scheme and employ weight decay to expedite the convergence rate. These techniques are aligned with our differential privacy analysis and do not increase privacy loss. We derive the algorithm in this section, omitting the subscript d for simplicity.

For each iteration i , we have:

$$\begin{aligned} \mathbf{W}^{(i+1)} &= \mathbf{W}^{(i)} - \eta \nabla_{\mathbf{W}} f(\mathbf{W}) + \mathcal{N}(0, 2\eta \cdot o(k, j) \mathbf{I}) \\ &= \mathbf{W}^{(i)} + \eta \left(\mathbf{u}^T \mathbf{x} - \theta^{(i)} \mathbf{x}^T \mathbf{x} \right) + \mathcal{N}(0, 2\eta \cdot o(k, j) \mathbf{I}) \\ &= \mathbf{W}^{(i)} (\mathbf{I} - \eta \mathbf{x}^T \mathbf{x}) + \eta \mathbf{u}^T \mathbf{x} + \mathcal{N}(0, 2\eta \cdot o(k, j) \mathbf{I}) \end{aligned} \quad (15)$$

where $\nabla_{\mathbf{W}} f(\mathbf{W}) = -(\mathbf{u}^T \mathbf{x} - \mathbf{u}^{(i)} \mathbf{x}^T \mathbf{x})$. We could regard the $(\mathbf{I} - \eta \mathbf{x}^T \mathbf{x})^{-1}$ as a weight decay term with coefficient $\mathbf{x}^T \mathbf{x}$. In privacy loss analysis, we could regard the weight decay term as a proximal operator with $L_T = \rho^2$. Hence, if $L_T \leq \rho^2 \leq 1$, we consider ignore this term because it will not increase the privacy loss. Therefore, we have:

$$\mathbf{W}^{(i+1)} = \mathbf{W}^{(i)} - \eta \mathbf{u}^T \mathbf{x} + \mathcal{N}(0, 2\eta \cdot o(k, j) \mathbf{I}) \quad (16)$$

Furthermore, since $(\mathbf{I} + \eta \mathbf{x}^T \mathbf{x})^{-1} \leq 1$, it does not increase the privacy loss either. Subsequently, we scale down the entire update scheme:

$$\mathbf{W}^{(i+1)} = (\mathbf{W}^{(i)} - \eta \mathbf{u}^T \mathbf{x} + \mathcal{N}(0, 2\eta \cdot o(k, j) \mathbf{I})) \cdot (\mathbf{I} + \eta \mathbf{x}^T \mathbf{x})^{-1} \quad (17)$$

Given that $(\mathbf{I} + \eta \mathbf{x}^T \mathbf{x})^{-1} \leq 1$, the privacy loss remains unaffected. The rationale for transforming the original update scheme to (17) is that it is the close form of the original sub-problem:

$$\mathbf{W} \leftarrow \arg \min_{\mathbf{W}'_d} \langle f(\mathbf{W}), \mathbf{W}' - \mathbf{W} \rangle + \frac{1}{2\eta} \|\mathbf{W}' - \mathbf{W}\|_F^2 \quad (18)$$

In practice, employing the update schemes (17) is more convenient because the linear approximation form (15) typically requires some iterations to reach the optimal value of each sub-problem. However, the linear approximation format is more advantageous in privacy loss analysis.

More Complicated Neural Architectures: Although we discuss feed forward neural networks as defined in (3) to derive the training algorithms in this section. We believe that neural networks with more complicated architectures can be included under this framework by proper formulation. For example, we consider adding one shortcut connection between the k_s -th layer to the k_d -th layer with the weight parameter \mathbf{S} , which is very popular in architectures like residual networks, the corresponding optimization problem will be as shown below:

$$\begin{aligned} \min_{\mathbf{W}} \mathcal{L}(\mathbf{W}, \mathbf{x}_0) &\stackrel{\text{def}}{=} \mathcal{R}(\mathbf{W}_D \mathbf{x}_D, y) + r(\mathbf{W}) \\ \text{s.t. } \mathbf{x}_{d+1} &= \sigma_d(\mathbf{W}_d \mathbf{x}_d), \quad d = 0, \dots, D-1 \text{ and } d \neq k_d \\ \mathbf{x}_{k_d+1} &= \sigma_{k_d}(\mathbf{W}_{k_d} \mathbf{x}_{k_d} + \mathbf{S} \sigma_{k_s}(\mathbf{W}_{k_s} \mathbf{x}_{k_s})) \end{aligned} \quad (19)$$

In this context, we can follow a similar methodology as in Section 3.2 and obtain the following Lagrangian function:

$$\begin{aligned} \mathcal{F}(\mathbf{W}, \mathbf{x}, \mathbf{u}) &= \mathcal{R}(\mathbf{W}_D \mathbf{x}_D, y) + \frac{\gamma}{2} \|\mathbf{u}_{k_d} - \mathbf{W}_{k_d} \mathbf{x}_{k_d} - \mathbf{S} \mathbf{x}_{k_s+1}\|^2 + \frac{\gamma}{2} \|\mathbf{x}_{k_d+1} - \sigma_{k_d}(\mathbf{u}_{k_d})\|^2 \\ &\quad + \frac{\gamma}{2} \sum_{d=0, d \neq k_d}^{D-1} (\|\mathbf{x}_{d+1} - \sigma_d(\mathbf{u}_d)\|^2 + \|\mathbf{u}_d - \mathbf{W}_d \mathbf{x}_d\|^2) + r(\mathbf{W}) \end{aligned} \quad (20)$$

As we can see, \mathcal{F} defined in Equation (20) is also a multi-convex function and we can follow a similar algorithm to the one discussed in this section to obtain a neural network with shortcut connections with DP guarantees under the hidden state assumption. We leave more discussions for general neural architectures as future works.

C Privacy Loss Analysis

C.1 Proof of Lemma 4.1

Proof. Based on the definition of Lipschitz continuity, we have:

$$\left\| \frac{\partial F(\boldsymbol{\theta})}{\partial \boldsymbol{\theta}} \right\| = \left\| 1 - \eta \nabla^2 f(\boldsymbol{\theta}) \right\|$$

We can bound the $\left\| \frac{\partial F(\boldsymbol{\theta})}{\partial \boldsymbol{\theta}} \right\|$ by control the learning rate η . More specifically, by imposing the constraint $\tilde{\eta} = \min \left\{ \frac{\kappa}{\|\nabla^2 f(\boldsymbol{\theta})\|}, \eta \right\}$ to bound the gradient $\frac{\partial F(\boldsymbol{\theta})}{\partial \boldsymbol{\theta}}$, it follows that $L_F \leq \max\{|1 - \kappa|, |1 - \eta\beta|\}$. The adaptive learning rate $\tilde{\eta}$ can be translated to a gradient clipping format: $\tilde{\nabla} f(\boldsymbol{\theta}) = \min \left\{ \frac{\kappa \nabla f(\boldsymbol{\theta})}{\|\nabla^2 f(\boldsymbol{\theta})\|}, \nabla f(\boldsymbol{\theta}) \right\}$

□

C.2 Proof of Lemma 4.2

Proof. Let $\tilde{\boldsymbol{\theta}}_1 = \text{Prox}_{\eta, r}(\boldsymbol{\theta}_1)$ and $\tilde{\boldsymbol{\theta}}_2 = \text{Prox}_{\eta, r}(\boldsymbol{\theta}_2)$, we then have the following inequalities based on the optimality:

$$\begin{aligned} r(\tilde{\boldsymbol{\theta}}_1) + \frac{1}{2\eta} \left\| \tilde{\boldsymbol{\theta}}_1 - \boldsymbol{\theta}_1 \right\|_2^2 &\leq r\left(\frac{\tilde{\boldsymbol{\theta}}_1 + \tilde{\boldsymbol{\theta}}_2}{2}\right) + \frac{1}{2\eta} \left\| \frac{\tilde{\boldsymbol{\theta}}_1 + \tilde{\boldsymbol{\theta}}_2}{2} - \boldsymbol{\theta}_1 \right\|_2^2 \\ r(\tilde{\boldsymbol{\theta}}_2) + \frac{1}{2\eta} \left\| \tilde{\boldsymbol{\theta}}_2 - \boldsymbol{\theta}_2 \right\|_2^2 &\leq r\left(\frac{\tilde{\boldsymbol{\theta}}_1 + \tilde{\boldsymbol{\theta}}_2}{2}\right) + \frac{1}{2\eta} \left\| \frac{\tilde{\boldsymbol{\theta}}_1 + \tilde{\boldsymbol{\theta}}_2}{2} - \boldsymbol{\theta}_2 \right\|_2^2 \end{aligned} \quad (21)$$

Based on the convexity of the function r , we have $2r\left(\frac{\tilde{\boldsymbol{\theta}}_1 + \tilde{\boldsymbol{\theta}}_2}{2}\right) \leq r(\tilde{\boldsymbol{\theta}}_1) + r(\tilde{\boldsymbol{\theta}}_2)$. Summing this inequality and the ones in (21), we obtain the following inequality.

$$\left\| \tilde{\boldsymbol{\theta}}_1 - \boldsymbol{\theta}_1 \right\|_2^2 + \left\| \tilde{\boldsymbol{\theta}}_2 - \boldsymbol{\theta}_2 \right\|_2^2 \leq \left\| \frac{\tilde{\boldsymbol{\theta}}_1 + \tilde{\boldsymbol{\theta}}_2}{2} - \boldsymbol{\theta}_1 \right\|_2^2 + \left\| \frac{\tilde{\boldsymbol{\theta}}_1 + \tilde{\boldsymbol{\theta}}_2}{2} - \boldsymbol{\theta}_2 \right\|_2^2$$

We simplify the inequality above and obtain $\|\tilde{\boldsymbol{\theta}}_2 - \tilde{\boldsymbol{\theta}}_1\|_2^2 \leq 2\langle \tilde{\boldsymbol{\theta}}_2 - \tilde{\boldsymbol{\theta}}_1, \boldsymbol{\theta}_2 - \boldsymbol{\theta}_1 \rangle$. Since $\langle \tilde{\boldsymbol{\theta}}_2 - \tilde{\boldsymbol{\theta}}_1, \boldsymbol{\theta}_2 - \boldsymbol{\theta}_1 \rangle \leq \|\tilde{\boldsymbol{\theta}}_2 - \tilde{\boldsymbol{\theta}}_1\|_2 \|\boldsymbol{\theta}_2 - \boldsymbol{\theta}_1\|_2$, so we have $\|\tilde{\boldsymbol{\theta}}_2 - \tilde{\boldsymbol{\theta}}_1\|_2 \leq 2\|\boldsymbol{\theta}_2 - \boldsymbol{\theta}_1\|_2$. □

C.3 Proof of Theorem C.2

For proof completeness, we first provide the formal definition of Log-Sobolev Inequality (LSI).

Definition C.1. (*Log-Sobolev Inequality Vempala and Wibisono [2019]*) A distribution ν over \mathbb{R}^d satisfies log-Sobolev inequality (LSI) with a constant c if \forall smooth function $g : \mathbb{R}^d \rightarrow \mathbb{R}$ with $\mathbb{E}_{\theta \sim \nu}[g^2(\theta)] < +\infty$,

$$\mathbb{E}_{\theta \sim \nu}[g^2(\theta) \log(g^2(\theta))] - \mathbb{E}_{\theta \sim \nu}[g^2(\theta)] \log \mathbb{E}_{\theta \sim \nu}[g^2(\theta)] \leq \frac{2}{c} \mathbb{E}_{\theta \sim \nu}[\|\nabla g(\theta)\|_2^2] \quad (22)$$

Then, we go to the formal proof of Theorem C.2.

Theorem C.2. (*Rate of RDP*) Let μ, ν be two distributions on \mathbb{R}^d . $F, T : \mathbb{R}^d \rightarrow \mathbb{R}^d$ are measurable mappings. We use $p_t(\theta)$ and $p'_t(\theta)$ to represent the probability density functions of $F_{\#}(\mu) * \mathcal{N}(0, 2t \cdot o(k, j) \cdot \mathbb{I}_d)$ and $F_{\#}(\nu) * \mathcal{N}(0, 2t \cdot o(k, j) \cdot \mathbb{I}_d)$. In addition, we use $h_t(\theta)$ and $h'_t(\theta)$ to represent the probability density function of $T_{\#}(F_{\#}(\mu) * \mathcal{N}(0, 2t \cdot o(k, j) \cdot \mathbb{I}_d))$ and $T_{\#}(F_{\#}(\nu) * \mathcal{N}(0, 2t \cdot o(k, j) \cdot \mathbb{I}_d))$. Furthermore, we use P to represent the probability transition function by the mapping $T_{\#}$, i.e., $h_t(\theta) = P(p_t(\theta))$ and $h'_t(\theta) = P(p'_t(\theta))$ are composition functions. If μ, ν satisfy log-sobolev inequality (LSI) with constant c , and if the mappings F, T are L_F, L_T -Lipschitz continuous, P is a linear function, then for any $\alpha > 1$, we have the following bound for the Rényi divergence of order α between $h_t(\theta)$ and $h'_t(\theta)$:

$$\frac{\partial}{\partial t} R_{\alpha}(h_t(\theta) \| h'_t(\theta)) \leq -2c_t \cdot o(k, j) \cdot \left(\frac{R_{\alpha}(h_t(\theta) \| h'_t(\theta))}{\alpha} + (\alpha - 1) \frac{\partial}{\partial \alpha} R_{\alpha}(h_t(\theta) \| h'_t(\theta)) \right) \quad (23)$$

where $c_t = \left(\frac{L_F^2}{c} + 2t \cdot o(k, j) \right)^{-1} / L_T^2$.

Proof. Denote $E_{\alpha}(h_t(\theta) \| h'_t(\theta)) = \int h'_t(\theta) \cdot \frac{h_t(\theta)^{\alpha}}{h'_t(\theta)^{\alpha}} d\theta$ to be the moment of the likelihood ratio function, then

$$R_{\alpha}(h_t(\theta) \| h'_t(\theta)) = \frac{1}{\alpha - 1} \log E_{\alpha}(h_t(\theta) \| h'_t(\theta)) \quad (24)$$

We compute the rate of Rényi divergence with regard to t as follows:

$$\begin{aligned} \frac{\partial R_{\alpha} h_t(\theta) \| h'_t(\theta)}{\partial t} &= \frac{1}{\alpha - 1} \log E_{\alpha}(h_t(\theta) \| h'_t(\theta)) \\ &= \frac{1}{(\alpha - 1) E_{\alpha}(h_t(\theta) \| h'_t(\theta))} \cdot \frac{\partial}{\partial t} \left(\int \frac{h_t(\theta)^{\alpha}}{h'_t(\theta)^{\alpha-1}} d\theta \right) \end{aligned} \quad (25)$$

By exchanging the order of derivative and integration since they are with respect to different variables, we have:

$$\begin{aligned} \frac{\partial R_{\alpha}(h_t(\theta) \| h'_t(\theta))}{\partial t} &= \frac{1}{(\alpha - 1) E_{\alpha}(h_t(\theta) \| h'_t(\theta))} \cdot \\ &\quad \int \left(\alpha \cdot \frac{h_t(\theta)^{\alpha-1}}{h'_t(\theta)^{\alpha-1}} \cdot \frac{\partial h_t(\theta)}{\partial p_t(\theta)} \cdot \frac{\partial p_t(\theta)}{\partial t} - (\alpha - 1) \cdot \frac{h_t(\theta)^{\alpha}}{h'_t(\theta)^{\alpha}} \cdot \frac{\partial h'_t(\theta)}{\partial p'_t(\theta)} \cdot \frac{\partial p'_t(\theta)}{\partial t} \right) d\theta \end{aligned} \quad (26)$$

Since the $\mu * \mathcal{N}(0, 2t \cdot o(k, j) \cdot \mathbb{I}_d)$ and $\nu * \mathcal{N}(0, 2t \cdot o(k, j) \cdot \mathbb{I}_d)$ are heat flow at time $t \in [0, o(k, j)]$. Therefore $p_t(\theta)$ and $p'_t(\theta)$ satisfy the following Fokker-Planck equations [Kadanoff, 2000].

$$\frac{\partial p_t(\theta)}{\partial t} = o(k, j) \Delta p_t(\theta), \quad \frac{\partial p'_t(\theta)}{\partial t} = o(k, j) \Delta p'_t(\theta) \quad (27)$$

Then Equation (26) can be written as

$$\begin{aligned} \frac{\partial R_{\alpha}(h_t(\theta) \| h'_t(\theta))}{\partial t} &= \frac{o(k, j)}{(\alpha - 1) E_{\alpha}(h_t(\theta) \| h'_t(\theta))} \cdot \\ &\quad \int \left(\alpha \cdot \frac{h_t(\theta)^{\alpha-1}}{h'_t(\theta)^{\alpha-1}} \cdot \frac{\partial h_t(\theta)}{\partial p_t(\theta)} \cdot \Delta p_t(\theta) \right. \\ &\quad \left. - (\alpha - 1) \cdot \frac{h_t(\theta)^{\alpha}}{h'_t(\theta)^{\alpha}} \cdot \frac{\partial h'_t(\theta)}{\partial p'_t(\theta)} \cdot \Delta p'_t(\theta) \right) d\theta \end{aligned} \quad (28)$$

We apply Green's first identity to further simplify the equation above:

$$\begin{aligned}
\int \alpha \cdot \frac{h_t(\boldsymbol{\theta})^{\alpha-1}}{h'_t(\boldsymbol{\theta})^{\alpha-1}} \cdot \frac{\partial h_t(\boldsymbol{\theta})}{\partial p_t(\boldsymbol{\theta})} \cdot \Delta p_t(\boldsymbol{\theta}) d\boldsymbol{\theta} &= - \int \nabla \left(\alpha \cdot \frac{h_t(\boldsymbol{\theta})^{\alpha-1}}{h'_t(\boldsymbol{\theta})^{\alpha-1}} \cdot \frac{\partial h_t(\boldsymbol{\theta})}{\partial p_t(\boldsymbol{\theta})} \right) \cdot \nabla p_t(\boldsymbol{\theta}) d\boldsymbol{\theta} \\
&= -\alpha \int \nabla \left(\frac{h_t(\boldsymbol{\theta})^{\alpha-1}}{h'_t(\boldsymbol{\theta})^{\alpha-1}} \right) \cdot \frac{\partial h_t(\boldsymbol{\theta})}{\partial p_t(\boldsymbol{\theta})} \cdot \nabla p_t(\boldsymbol{\theta}) d\boldsymbol{\theta} \\
&= -\alpha \int \nabla \left(\frac{h_t(\boldsymbol{\theta})^{\alpha-1}}{h'_t(\boldsymbol{\theta})^{\alpha-1}} \right) \cdot \nabla h_t(\boldsymbol{\theta}) d\boldsymbol{\theta}
\end{aligned} \tag{29}$$

To avoid confusion, all ∇ operators represent the derivative with respect to $\boldsymbol{\theta}$. Note that $h_t(\boldsymbol{\theta}) = P(p_t(\boldsymbol{\theta}))$ and P is a linear function, so $\frac{\partial h_t(\boldsymbol{\theta})}{\partial p_t(\boldsymbol{\theta})}$ is a constant. This is why we can move the term $\frac{\partial h_t(\boldsymbol{\theta})}{\partial p_t(\boldsymbol{\theta})}$ outside the ∇ operator.

Using the same technique, we can bound the second term of Equation (28):

$$\int -(\alpha - 1) \cdot \frac{h_t(\boldsymbol{\theta})^\alpha}{h'_t(\boldsymbol{\theta})^\alpha} \cdot \frac{\partial h_t(\boldsymbol{\theta})}{\partial p_t(\boldsymbol{\theta})} \cdot \Delta p'_t(\boldsymbol{\theta}) d\boldsymbol{\theta} = (\alpha - 1) \int \nabla \left(\frac{h_t(\boldsymbol{\theta})^\alpha}{h'_t(\boldsymbol{\theta})^\alpha} \right) \cdot \nabla h'_t(\boldsymbol{\theta}) d\boldsymbol{\theta} \tag{30}$$

Plug Equation (29) and (30) into Equation (28), we have the following equation:

$$\begin{aligned}
\frac{\partial R_\alpha(h_t(\boldsymbol{\theta})\|h'_t(\boldsymbol{\theta}))}{\partial t} &= \frac{\alpha \cdot o(k, j)}{E_\alpha(h_t(\boldsymbol{\theta})\|h'_t(\boldsymbol{\theta}))} \cdot \left(\frac{1}{\alpha} \int \nabla \left(\frac{h_t(\boldsymbol{\theta})^\alpha}{h'_t(\boldsymbol{\theta})^\alpha} \right) \cdot \nabla h'_t(\boldsymbol{\theta}) d\boldsymbol{\theta} \right. \\
&\quad \left. - \frac{1}{\alpha - 1} \int \nabla \left(\frac{h_t(\boldsymbol{\theta})^{\alpha-1}}{h'_t(\boldsymbol{\theta})^{\alpha-1}} \right) \cdot \nabla h_t(\boldsymbol{\theta}) d\boldsymbol{\theta} \right) \\
&= \frac{\alpha \cdot o(k, j)}{E_\alpha(h_t(\boldsymbol{\theta})\|h'_t(\boldsymbol{\theta}))} \left(\int \frac{h_t(\boldsymbol{\theta})^{\alpha-1}}{h'_t(\boldsymbol{\theta})^{\alpha-1}} \cdot \left\langle \nabla \left(\frac{h_t(\boldsymbol{\theta})}{h'_t(\boldsymbol{\theta})} \right), \nabla h'_t(\boldsymbol{\theta}) \right\rangle d\boldsymbol{\theta} \right. \\
&\quad \left. - \int \frac{h_t(\boldsymbol{\theta})^{\alpha-2}}{h'_t(\boldsymbol{\theta})^{\alpha-2}} \cdot \left\langle \nabla \left(\frac{h_t(\boldsymbol{\theta})}{h'_t(\boldsymbol{\theta})} \right), \nabla h_t(\boldsymbol{\theta}) \right\rangle d\boldsymbol{\theta} \right) \\
&= -\frac{\alpha \cdot o(k, j)}{E_\alpha(h_t(\boldsymbol{\theta})\|h'_t(\boldsymbol{\theta}))} \int \frac{h_t(\boldsymbol{\theta})^{\alpha-2}}{h'_t(\boldsymbol{\theta})^{\alpha-2}} \cdot \left\langle \nabla \left(\frac{h_t(\boldsymbol{\theta})}{h'_t(\boldsymbol{\theta})} \right), \nabla \left(\frac{h_t(\boldsymbol{\theta})}{h'_t(\boldsymbol{\theta})} \right) \right\rangle h'_t(\boldsymbol{\theta}) d\boldsymbol{\theta} \\
&\stackrel{\text{def}}{=} -\alpha \cdot o(k, j) \cdot \frac{I_\alpha(h_t(\boldsymbol{\theta})\|h'_t(\boldsymbol{\theta}))}{E_\alpha(h_t(\boldsymbol{\theta})\|h'_t(\boldsymbol{\theta}))}
\end{aligned} \tag{31}$$

where we define $I_\alpha(h_t(\boldsymbol{\theta})\|h'_t(\boldsymbol{\theta})) = \int \frac{h_t(\boldsymbol{\theta})^{\alpha-2}}{h'_t(\boldsymbol{\theta})^{\alpha-2}} \cdot \left\langle \nabla \left(\frac{h_t(\boldsymbol{\theta})}{h'_t(\boldsymbol{\theta})} \right), \nabla \left(\frac{h_t(\boldsymbol{\theta})}{h'_t(\boldsymbol{\theta})} \right) \right\rangle \cdot h'_t(\boldsymbol{\theta}) d\boldsymbol{\theta} = \mathbb{E}_{\boldsymbol{\theta} \sim h'_t} \left(\frac{h_t(\boldsymbol{\theta})^\alpha}{h'_t(\boldsymbol{\theta})^\alpha} \left\| \nabla \log \frac{h_t(\boldsymbol{\theta})}{h'_t(\boldsymbol{\theta})} \right\|_2^2 \right)$.

Based on Vempala and Wibisono [2019, Lemma 16, Lemma 17], we can conclude $h_t(\boldsymbol{\theta})$ and $h'_t(\boldsymbol{\theta})$ satisfy log-Sobolev inequality with a constant $c_t = \left(\frac{L_F^2}{c} + 2t \cdot o(k, j) \right)^{-1} / L_T^2$. In this regard, we can utilize Ye and Shokri [2022, Lemma D.1] and Vempala and Wibisono [2019, Lemma 5] to bound $\frac{I_\alpha(h_t(\boldsymbol{\theta})\|h'_t(\boldsymbol{\theta}))}{E_\alpha(h_t(\boldsymbol{\theta})\|h'_t(\boldsymbol{\theta}))}$ as follows:

$$\frac{I_\alpha(h_t(\boldsymbol{\theta})\|h'_t(\boldsymbol{\theta}))}{E_\alpha(h_t(\boldsymbol{\theta})\|h'_t(\boldsymbol{\theta}))} \geq \frac{2c_t}{\alpha^2} \cdot R_\alpha(h_t(\boldsymbol{\theta})\|h'_t(\boldsymbol{\theta})) + \frac{2c_t}{\alpha^2} \cdot \alpha(\alpha - 1) \frac{\partial}{\partial \alpha} R_\alpha(h_t(\boldsymbol{\theta})\|h'_t(\boldsymbol{\theta})) \tag{32}$$

Combine Inequality (32) with Equation 31, we conclude the proof. \square

The theorem C.2 bound the rate of Rényi divergence follows Ye and Shokri [2022], Vempala and Wibisono [2019]. One assumption in Theorem C.2 is P being a linear function. The function P depicts the change of the probability density functions before and after the proximal operator. For the three typical regularization function r discussed previously, including no regularization, l_2 regularization and l_1 regularization, it is clear that all their corresponding P functions are linear. In addition, the Lipschitz continuity of function F and T is guaranteed in Lemma 4.1 and Lemma 4.2, respectively. Therefore, we can conclude that the assumptions in Theorem C.2 are not restrictive.

Theorem C.2 considers the recursive privacy dynamics during one step of noisy mini-batch proximal gradient descent in (6). In the corollary 4.5, we apply the Theorem C.2 in the context of differential privacy. Under Assumption 4.4, we can then apply Theorem C.2 to the case of two neighboring datasets and obtain the following corollary.

C.4 Proof of Theorem 4.6

Before proving the main theorem, we first calculate the LSI constant sequence in Algorithm 1.

Lemma C.3. (*LSI constant sequence in Algorithm 1*) For each layer's update scheme in Algorithm 1 with a batch size of b , if the update function $F(\theta) = \theta - \eta \nabla f(\theta)$ and the proximal operator $T(\theta) = \text{Prox}_{\eta, r}$ are Lipschitz continuous with Lipschitz constant L_F and L_T , respectively, then the distribution of parameter θ_k^j in the j -th iteration of the k -th epoch satisfies c_k^j log-Sobolev inequality (LSI) and the constant c_k^j is calculated by:

$$c_k^j = \frac{1}{2\eta L_T^2} \left(\sum_{k'=0}^{k-1} \sum_{j'=0}^{n/b-1} o(k', j') (L_F L_T)^{2((k-k')(n/b)-j'+j-1)} + \sum_{j'=0}^{j-1} o(k, j') (L_F L_T)^{2(j-j'-1)} \right)^{-1}$$

Proof. Based on Definition C.1, the LSI constant of the Gaussian distribution $\mathcal{N}(0, 2t \cdot o(k, j))$ is $\frac{1}{2t \cdot o(k, j)}$.

Then, Using the LSI under Lipschitz mapping [Vempala and Wibisono, 2019, lemma 16] and Gaussian convolution [Vempala and Wibisono, 2019, lemma 17], we have $\frac{1}{c_k^j} = \frac{L^2}{c_{k-1}^j} + 2\eta L_T^2 \cdot o(k, j-1)$ where $L = L_F L_T$ for notation simplicity. By applying this equation iteratively via j and k , we obtain:

$$\begin{aligned} \frac{1}{c_k^j} &= \frac{L^{2j}}{c_k^0} + 2\eta L_T^2 \sum_{j'=0}^{j-1} o(k, j') L^{2(j-j'-1)} \\ &= \frac{L^{2(k \cdot n/b + j)}}{c_0^0} + 2\eta L_T^2 \left(\sum_{k'=0}^{k-1} \sum_{j'=0}^{n/b-1} o(k', j') L^{2((k-k')(n/b)-j'+j-1)} + \sum_{j'=0}^{j-1} o(k, j') L^{2(j-j'-1)} \right) \end{aligned}$$

Because the initialization is point distribution around θ_0 , θ_0^0 satisfies the log-Sobolev inequality with constant $c_0^0 = \infty$, and the lemma is then proved. \square

We now return to Theorem 4.6 and provide the complete proof below.

Proof. We denote θ_k^j and $\theta_k'^j$ as the intermediate parameters in the j -th iteration of the k -th epoch in Algorithm 1 when using two neighboring datasets D and D' . In addition, we use $\varepsilon_k^j(\alpha) = R_\alpha(\theta_k^j || \theta_k'^j)$ to represent the Rényi divergence of order α between them. In this regard, it is clear that $\varepsilon_0^0(\alpha) = 0$.

Without the loss of generality, we assume that the only different data point is in the j_0 -th batch. Therefore, the privacy bound after K epochs can be decomposed into three parts by using 4.5: 1) the first $j_0 - 1$ mini-batch updates in the first epoch; 2) the remaining mini-batch updates in the first epoch; 3) the rest epochs.

In the first stage, we have $\forall j \in \{0, 1, \dots, j_0 - 1\}$ and $\forall \alpha > 1, \varepsilon_0^j(\alpha) = 0$ based on Lemma 4.5.

In the second stage, we have $\forall \alpha, \frac{\varepsilon_0^{j_0}(\alpha)}{\alpha} \leq \frac{\eta S_g^2}{4b^2 \cdot o(0, j_0)}$. Then we bound the privacy loss in the end of the first epoch by the following inequality. Note that, this inequality is applicable for any $\alpha > 1$.

$$\forall \alpha > 1, \quad \frac{\varepsilon_0^{n/b-1}(\alpha)}{\alpha} \leq \frac{\eta S_g^2}{4b^2 \cdot o(0, j_0)} \prod_{j=j_0+1}^{n/b-1} \left(1 + \frac{c_0^j \cdot 2\eta \cdot o(0, j)}{L_F^2} \right)^{-1/L_T^2} \quad (33)$$

In the third stage, we first consider the second epoch, especially the j_0 -th iteration and the last iteration. Based on Lemma 4.5, we have the following inequalities:

$$\begin{aligned}
\frac{\varepsilon_1^{j_0}(\alpha)}{\alpha} &\leq \frac{\varepsilon_1^{-1}(\alpha')}{\alpha'} \prod_{j=0}^{j_0-1} \left(1 + \frac{c_1^j \cdot 2\eta \cdot o(1, j)}{L_F^2}\right)^{-1/L_T^2} + \frac{\eta S_g^2}{4b^2 \cdot o(1, j_0)} \\
\frac{\varepsilon_1^{n/b-1}(\alpha)}{\alpha} &\leq \frac{\varepsilon_1^{j_0}(\alpha'')}{\alpha''} \prod_{j=j_0+1}^{n/b-1} \left(1 + \frac{c_1^j \cdot 2\eta \cdot o(1, j)}{L_F^2}\right)^{-1/L_T^2} \\
&\leq \left(\frac{\varepsilon_1^{-1}(\alpha''')}{\alpha'''} \prod_{j=0}^{j_0-1} \left(1 + \frac{c_1^j \cdot 2\eta \cdot o(1, j)}{L_F^2}\right)^{-1/L_T^2} + \frac{\eta S_g^2}{4b^2 \cdot o(1, j_0)} \right) \\
&\quad \cdot \prod_{j=j_0+1}^{n/b-1} \left(1 + \frac{c_1^j \cdot 2\eta \cdot o(1, j)}{L_F^2}\right)^{-1/L_T^2}
\end{aligned} \tag{34}$$

Here, we use ε_1^{-1} to represent the privacy bound before the first iteration of the second epoch. It is clear that $\varepsilon_1^{-1} = \varepsilon_0^{n/b-1}$. In addition, α' , α'' and α''' are the j_0 , $(n/b - 1 - j_0)$ and $(n/b - 1)$ fold mapping value of α under the repeated mapping $\alpha \leftarrow (\alpha - 1) \cdot \left(1 + \frac{c_1^j \cdot 2\eta \cdot o(1, j)}{L_F^2}\right)^{-1/L_T^2}$, respectively.

Considering inequality (33) holds for any $\alpha > 1$ and the fact $\alpha''' > 1$, we can then plug inequality (33) into inequality (34) and obtain the following inequality:

$$\begin{aligned}
\frac{\varepsilon_1^{n/b-1}(\alpha)}{\alpha} &\leq \frac{\eta S_g^2}{4b^2 \cdot o(0, j_0)} \prod_{j=j_0+1}^{n/b-1} \left(1 + \frac{c_0^j \cdot 2\eta \cdot o(0, j)}{L_F^2}\right)^{\frac{-1}{L_T^2}} \\
&\quad \prod_{j=0, j \neq j_0}^{n/b-1} \left(1 + \frac{c_1^j \cdot 2\eta \cdot o(1, j)}{L_F^2}\right)^{\frac{-1}{L_T^2}} + \frac{\eta S_g^2}{4b^2 \cdot o(1, j_0)} \prod_{j=j_0+1}^{n/b-1} \left(1 + \frac{c_1^j \cdot 2\eta \cdot o(1, j)}{L_F^2}\right)^{\frac{-1}{L_T^2}}
\end{aligned} \tag{35}$$

By recursively applying Equation (35), we can obtain the privacy bound of the whole training phase. For notation simplicity, we use $\Phi(k_1, k_2)$ to denote the RDP's decay rate between the k_1 -th epoch and the k_2 -th epoch.

$$\Phi(k_1, k_2) = \prod_{k=k_1}^{k_2-1} \prod_{j=0, j \neq j_0}^{n/b-1} \left(1 + \frac{c_k^j \cdot 2\eta \cdot o(k, j)}{L_F^2}\right)^{-1/L_T^2} \tag{36}$$

In Lemma C.3 we have $\frac{1}{c_k^{j+1}} = \frac{L_F^2 L_T^2}{c_k^j} + 2\eta L_T^2 \cdot o(k, j)$ based on the LSI under Lipschitz mapping [Vempala and Wibisono, 2019, Lemma 16] and Gaussian convolution [Vempala and Wibisono, 2019, Lemma 17], so $1 + \frac{c_k^j \cdot 2\eta \cdot o(k, j)}{L_F^2} = \frac{c_k^j}{c_k^{j+1}} \cdot \frac{1}{L_F^2 L_T^2}$. Therefore, Equation (36) can be further simplified as follows:

$$\Phi(k_1, k_2) = \left(\frac{c_{k_1}^0}{c_{k_2-1}^{n/b-1}} \left(\frac{1}{L_F^2 L_T^2} \right)^{(n/b-1)(k_2-k_1)} \prod_{k=k_1}^{k_2-1} \frac{c_k^{j_0+1}}{c_k^{j_0}} \right)^{-1/L_T^2} \tag{37}$$

Therefore, we can obtain the privacy bound after K epochs as follows:

$$\begin{aligned}
\frac{\varepsilon_K^{n/b-1}(\alpha)}{\alpha} &\leq \sum_{k=0}^{K-1} \frac{\eta S_g^2}{4b^2 \cdot o(k, j_0)} \cdot \Phi(k+1, K) \cdot \prod_{j=j_0+1}^{n/b-1} \left(1 + \frac{c_k^j \cdot 2\eta \cdot o(k, j)}{L_F^2}\right)^{-1/L_T^2} \\
&= \sum_{k=0}^{K-1} \frac{\eta S_g^2}{4b^2 \cdot o(k, j_0)} \left(\frac{c_k^{j_0+1}}{c_K^{n/b-1}} \left(\frac{1}{L_F^2 L_T^2} \right)^{(n/b-1)(K-k)-j_0} \prod_{l=k}^K \frac{c_l^{j_0+1}}{c_l^{j_0}} \right)^{-1/L_T^2}
\end{aligned} \tag{38}$$

Note that the right-hand side of inequality (38) depends on j_0 as well. We now explicitly rewrite $\varepsilon_K^{n/b-1}(\alpha)$ as $\varepsilon_K^{n/b-1}(\alpha, j_0)$ and bound the value of $\varepsilon_K(\alpha)$ in a similar way to Ye and Shokri [2022, Theorem 4.2]:

$$\begin{aligned} \varepsilon_K(\alpha) &= \mathbb{E}_{j_0} \varepsilon_K^{n/b-1}(\alpha, j_0) = \frac{1}{\alpha-1} \log e^{(\alpha-1)\mathbb{E}_{j_0} \varepsilon_K^{n/b-1}} \\ &\leq \frac{1}{\alpha-1} \log \left(\mathbb{E}_{j_0} e^{(\alpha-1)\varepsilon_K^{n/b-1}} \right) = \frac{1}{\alpha-1} \log \left(\sum_{j_0=0}^{n/b-1} \frac{b}{n} \cdot e^{(\alpha-1)\varepsilon_K^{n/b-1}(\alpha, j_0)} \right) \end{aligned} \quad (39)$$

□

D Numerical Experiments

In this section, we first use several datasets to verify the utility of our algorithm and then show that the adaptive noise could provide better privacy-utility trade-off.

D.1 Utility verification

This section applies Algorithm 3 and Algorithm 4 to NMF and neural network training problems and aims to verify the utility of the DP-MBCD algorithm. In order to provide an intuitive comparison between our algorithm and DP-SGD, we also provide the utility of DP-SGD under the same privacy loss. However, it is crucial to note that direct comparisons of privacy loss can be misleading due to the differing threat models. Privacy loss under the hidden state assumption provides DP guarantees for the **distribution of published (final iteration) parameters**, whereas privacy loss under the composition theorem ensures DP guarantees for the **distribution of parameters at each iteration**. The theoretical connection between these two types of privacy loss remains an open question.

D.1.1 NMF with Synthetic Data

For NMF optimization problems, we use the relative error as the metric for the utility, which is defined as $\|\mathbf{XY} - \mathbf{M}\|_F / \|\mathbf{M}\|_F$, to evaluate algorithmic performance. We utilize synthetic data from Xu and Yin [2013]. More specifically, we first generate non-negative random matrix $\mathbf{X} \in \mathbb{R}^{1000 \times 10}$ and $\mathbf{Y} \in \mathbb{R}^{10 \times 200}$, and we have $\mathbf{M} = \mathbf{XY}$ where $\mathbf{M} \in \mathbb{R}^{1000 \times 200}$. Moreover, we have batch size $b \in \{50, 100, 200\}$, and RDP order $\alpha = 2$. For DP-MBCD, we fix the epoch number at 1000000, with $\kappa = 1.1$, $S_g = 1$ and $\sigma^2 = 0.001$. For DP-SGD, we first set a fixed privacy loss, then conduct a grid search for optimal results. Additionally, when the privacy budget $\varepsilon = +\infty$, we employ vanilla algorithms without privacy enhancement mechanisms, i.e., mini-batch coordinate descent (MCD) and stochastic gradient descent (SGD), and report their performance for references. We run both algorithms for 1000 iterations.

The results in relative error are summarized in Table 2 below. We run each experimental setting for 3 times, the average and standard deviations are reported accordingly. It is clear that MBCD has much better performance than DP-SGD under the same privacy budget. The observations in Table 2 not only validate the effectiveness of our proposed methods, but also indicate that hidden state assumption is more realistic than composition theorem in practice.

Batch Size	$\varepsilon = 0.42$		$\varepsilon = +\infty$	
	DPMBCD (HSA)	DPSGD (CT)	MBCD	SGD
50	0.033 (± 0.023)	0.654(± 0.053)	0.030(± 0.005)	0.035(± 0.011)
100	0.037 (± 0.027)	0.693(± 0.027)	0.015(± 0.012)	0.016(± 0.021)
200	0.047 (± 0.021)	0.712(± 0.013)	0.009 (± 0.003)	0.008(± 0.004)

Table 2: Relative Error(in % under 95% confidential interval) for DP-MBCD and DP-SGD

D.1.2 Neural Network Training

In neural network training problem, we apply our algorithms on MNIST and Adults, which are widely used in membership inference attacks, to show the validation of our algorithm. To accelerate the algorithm, we use a variant of the Algorithm 4 demonstrated in the Appendix B.2.2.

We employ a four-layer multilayer perceptron (MLP) model, where each layer consists of 1200 neurons. The activation function is ReLU, and we use the mean square error (MSE) as the loss function. To reduce the variance, we use data

augmentation to double the original dataset and set the batch size to 60000. Since this experiment primarily demonstrates the effectiveness of our algorithm, we provide a **fixed differential privacy setting** rather than different initial noise, which will be discussed in the next subsection. Hence, for DP-MBCD, we set calibrated noise $o(K, j) = 0.001$, layer-wise Lipschitz constant $\rho_d^2 = 1$, and the step size $\eta = 0.1$. We train models until converge because the privacy loss under fixed noise can also converge. For privacy loss accountant, we set $\delta = 10^{-5}$. For RDP order α , we use the binary search, which is the same as FastDPBu et al. [2023] library, to find the optimal α . We implement our algorithm with above setting on both MNIST dataset and FashionMNIST dataset. We use the variant of Algorithm 4 demonstrated in Appendix B.2.2 to accelerate the convergence.

For DP-SGD, we use the FastDP library Bu et al. [2023] with the auto-clipping mode, which normalize the gradient and add calibrate noise. Bu et al. [2024] shows that this mode could outperforms or matches the state-of-the-art. The auto clipping mechanism also simplify the super parameter choose. For vanilla DP-SGD, we need to carefully choose clipping threshold as well as learning rate, which make it more difficult to balance the privacy loss and utility. The epoch is 50 because the number of epoch is necessary for the privacy accountant of the DP-SGD algorithm. Moreover, the utility may be even worse when epoch is larger because it will add larger calibrated noise to the training gradient. Moreover, the learning rate is crucial for DP-SGD's utility and privacy loss accountant. In our experiment, we choose different learning rate for different architecture and dataset.

Dataset	Avg Acc (DP-MBCD)	Avg Acc (DP-SGD)	Architecture	ε with $\delta = 10^{-5}$
MNIST	94.63(± 0.68)	67.33(± 0.73),lr=0.2	MLP	0.0612
MNIST	96.36(± 0.42)	67.73(± 1.12),lr=0.1	LeNet	0.0765
Fashion-MNIST	82.82(± 0.80)	18.27(± 2.35),lr=0.01	MLP	0.0612
Fashion-MNIST	79.21(± 0.97)	60.62(± 0.17),lr=0.1	LeNet	0.0765

Table 3: The accuracy(in % under 95% confidential interval) for DP-MBCD and DP-SGD 50

D.1.3 Conclusion

The results from both problems indicate that our algorithm can converge effectively. Furthermore, the privacy loss under the hidden state assumption is significantly smaller than that under the composition theorem. In scenarios where the same level of privacy loss is maintained, the DP-SGD have bad performance due to excessive noise. This highlights the **fundamental differences** between the two types of privacy loss calculations.

One of the drawbacks of our algorithm is that Algorithm 3 requires more iteration times. For neural networks, the second-order gradient can be bounded by normalizing \mathbf{x} in equation 12, eliminating the need to control L_F via learning rate. However, for Algorithm 3, the gradient is clipped by the second-order gradient term. Thus, it needs more iterations to converge.

D.2 Utility-Privacy Trade-off

In this section, we run numerical simulations in this section to investigate the model's utility and privacy loss in different training phases when we use different distributions to sample calibrated noise.

The Madelon dataset was originally introduced as a challenging classification problem in the NIPS 2003 feature selection challenge [Guyon et al., 2004]. This synthetic dataset comprises 6000 instances, each with 20 features and belonging to one of the five classes. To ensure an unbiased evaluation, we divided the dataset into a training set, accounting for 80% of the data, and a testing set, containing the remaining 20%. The batch size is 960.

We employ a smaller with four layers, each of which has 200 neurons. The activation function is the commonly used ReLU function, and we use squared loss as the loss function. In addition, we set the layerwise Lipschitz constant $\rho = 1$ and the step size $\eta = 0.05$. To guarantee privacy, we applied Theorem 4.6 and employed the privacy loss calculation with $\alpha = 2$.

The experiment compares the algorithm's utility under different noise strategies: the constant strategy with $o(k, j) = 0.005$ and the decrease strategy with a linear decay rate of 0.00025 per epoch and final noise variance $o(K, j) = 0.002$. The decrease strategy is designed in a manner so that the privacy loss of both strategies will be approximately the same for the same number of epochs K . Based on the aforementioned setup, we train the model 40 times where the total number of epochs K varies from 10 to 40. We run the whole experiment 3 times and report both the average performance and the standard deviation. The results are demonstrated in Figure 3 and Table 4.

The experiment results validate the effectiveness of Algorithm 4. What's more, with proper settings of adaptive calibrated noise, the algorithm can demonstrate a better trade-off between the model's utility and privacy. For the

EPOCH	NOISE	PRIVACY LOSS	AVG ACC.
10	C	0.0251	50.00(± 2.59)
20	C	0.0290	70.09(± 2.64)
30	C	0.0274	82.78(± 1.69)
40	C	0.0256	89.68(± 0.89)
10	D	0.0109	48.20(± 3.36)
20	D	0.0141	72.65(± 1.56)
30	D	0.0178	85.98(± 0.64)
40	D	0.0252	92.20(± 0.48)

Table 4: The accuracy(in % under 95% confidential interval) and the privacy loss of Algorithm 4 when we use different noise strategies and train the model for different numbers of epochs. D means noise decrease scenario and C means noise constant scenario

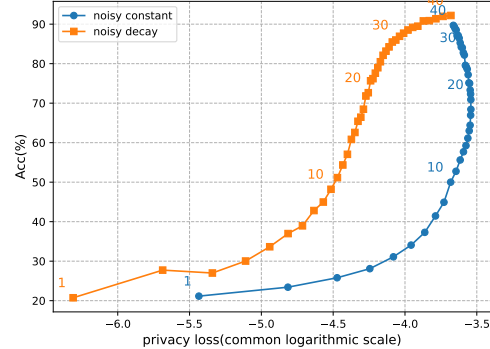


Figure 3: Relationship between model's utility and privacy loss under different noise strategies. For each noise strategy, we run Algorithm 4 for different numbers of epochs to plot the curve. The points are plotted in the order of epochs and we annotate some points aligned with the Table 4

examples in Table 4, we see higher utilities and lower privacy loss when we use adaptive calibrated noise. In Figure 3, the x -axis is the privacy loss while the y -axis is the utility, and the curve of adaptive calibrated noise above one of its counterparts in most cases. It shows that adaptive calibrated noise can provide better privacy utility trade-off than constant noise. However, since the privacy loss accountant methods proposed in Theorem 4.6 is highly depend on algorithm 1's hyper-parameters, how to design the adaptive noise strategy to guarantee a better trade-off is still very complex. We would like to defer it to future work.

E Privacy Bound Comparison with Ye and Shokri [2022]

In this section, we intend to provide an intuitive comparison between our privacy loss accountant bound (Theorem 4.6) and [Ye and Shokri, 2022, Corollary 5.3]. Comparing with our work, Ye and Shokri [2022]'s work requires strongly convexity coefficient to bound the Lipschitzness. In order to provide comparability, we set $\lambda = 1$ and $\eta = 0.05$ to guarantee two accountant methods have same $L_F = 0.95$. Moreover, we set batch size $b = 10$, data set $n = 90$, sensitivity $S_g = 1$, RDP order $\alpha = 6$. The Figure 4 illustrates the privacy loss for a strongly convex problem with different calibrated noise for our privacy loss accountant method and Ye and Shokri [2022]'s method. It is evident that our algorithm provides a tighter privacy loss bound than Ye and Shokri [2022].

The enhanced tightness of our bound is attributable to the comprehensive consideration of each epoch's privacy loss decreasing phase. Specifically, The Corollary 4.5 elucidates that when $i_0 \notin B_k^j$, the privacy loss will decrease exponentially. In our paper, the calibrated noise can be modified in each iteration, so we carefully derive each iteration's decreasing rate in equation (35).

In contrast, the paper by Ye and Shokri [2022] primarily focuses on presenting the convergence property while keeping the calibrated noise fixed. This leads them to approximate the overall privacy loss by neglecting part of the decreasing phase in each epoch. Specifically, in their equation (102) to (104), they simplified the decreasing rate by taking the upper bound. However, the exponential decrease term implies that even a minor approximation can lead to a significant difference. Consequently, our analysis demonstrates clearly superior accuracy compared to that of Ye and Shokri [2022].

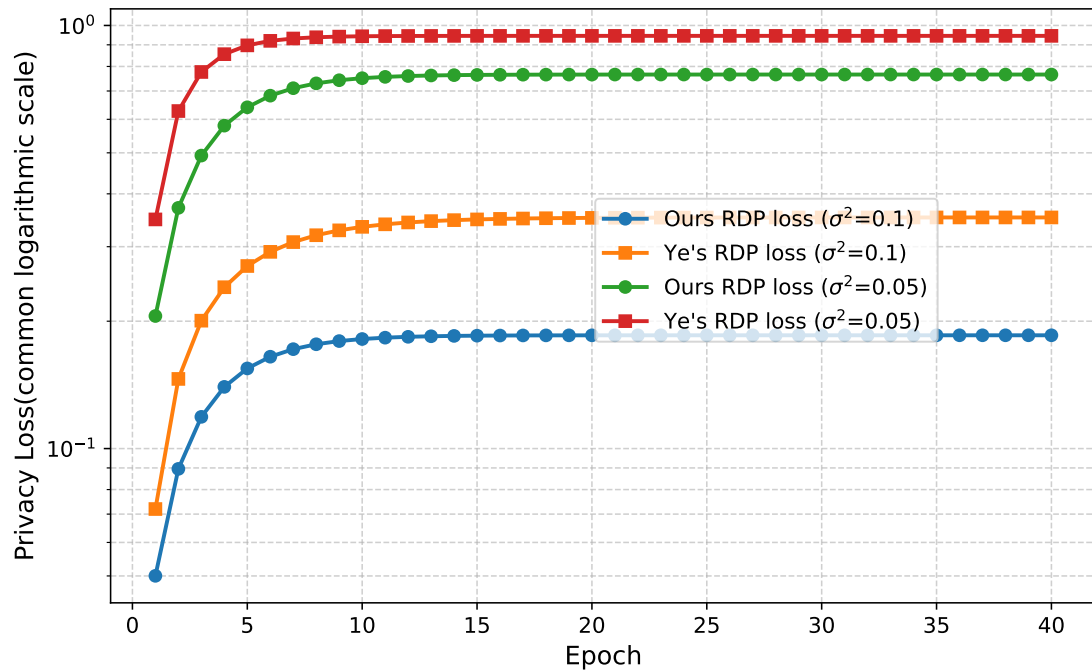


Figure 4: RDP loss comparison where common hyper-parameter settings are: learning rate $\eta = 0.1$, Lipschitz constant $L_F = 0.9$, batch size $b = 2$, data set $n = 40$, sensitivity $S_g = 1$, RDP order $\alpha = 10$